Copper(I) thiocyanate (CuSCN) as a hole-transport material for large-area opto/electronics

2015 Semicond. Sci. Technol. 30 104002

IOP Publishing Semiconductor Science and Technology
Semicond. Sci. Technol. **30** (2015) 104002 (21pp) doi:10.1088/0268-1242/30/10/104002

Copper(I) thiocyanate (CuSCN) as a hole-transport material for large-area opto/electronics

Nilushi Wijeyasinghe and Thomas D Anthopoulos

Department of Physics and Centre for Plastic Electronics, Blackett Laboratory, Imperial College London, London SW7 2BW, UK

E-mail: thomas.anthopoulos@imperial.ac.uk

Received 17 March 2015, revised 17 June 2015
Accepted for publication 1 July 2015
Published 24 August 2015

Abstract

Recent advances in large-area optoelectronics research have demonstrated the tremendous potential of copper(I) thiocyanate (CuSCN) as a universal hole-transport interlayer material for numerous applications, including transparent thin-film transistors, high-efficiency organic and hybrid organic-inorganic photovoltaic cells, and organic light-emitting diodes. CuSCN combines intrinsic hole-transport (p-type) characteristics with a large bandgap (>3.5 eV) which facilitates optical transparency across the visible to near infrared part of the electromagnetic spectrum. Furthermore, CuSCN is readily available from commercial sources while it is inexpensive and can be processed at low-temperatures using solution-based techniques. This unique combination of desirable characteristics makes CuSCN a promising material for application in emerging large-area optoelectronics. In this review article, we outline some important properties of CuSCN and examine its use in the fabrication of potentially low-cost optoelectronic devices. The merits of using CuSCN in numerous emerging applications as an alternative to conventional hole-transport materials are also discussed.

Keywords: copper thiocyanate, hole transport, transparent semiconductor, solar cells, OLEDs, transistors, hole mobility

(Some figures may appear in colour only in the online journal)

1. Introduction

Optically transparent semiconductors, which can be solution-processed at low temperatures over large-area substrates, are in great demand within the electronics industry. Hole-transporting (p-type) materials that fit this description can be utilized as hole injection, extraction and transport interlayers in various optoelectronic devices and systems. They are at present incorporated into numerous opto/electronic devices including organic light-emitting diodes (OLEDs) [1, 2], organic photovoltaics (OPV) [3], and hybrid organic-inorganic photovoltaic cells [4]. Thin-film transistors (TFTs) based on materials with the aforementioned properties are also required for large-area microelectronics applications such driving backplanes for optical displays [5–7]. In most cases, the hole mobilities of transparent intrinsic semiconductors (e.g. metal oxides) are inherently lower than the corresponding electron mobilities [8]. Such low hole mobilities primarily arise from the spatial overlap of electronic wavefunctions contributing to the hole-transporting valence band being smaller and the bands being less disperse. Furthermore, most intrinsic wide-bandgap semiconductors do not have an electronic or physical structure that facilitates successful acceptor doping in order to generate a surplus of mobile holes as the majority carriers. The result is thus a limited supply of transparent, high-mobility p-type systems, which poses a significant challenge to the advancement of optoelectronic technologies because optimum device performance requires high conductivity of both types of charge carriers. Therefore, it is essential to identify p-type materials that are capable of

meeting the increasing demand for faster operating frequencies and higher device efficiencies.

Common inorganic semiconductors, such as silicon, are crystalline solids in which the chemical bonding exhibits a permanent, strongly covalent character. Conversely, organic semiconductors (e.g. pentacene) are generally molecular solids, where strong (covalent) chemical bonds are only present within individual molecules. Weak atomic binding in the form of van der Waals forces, which includes non-permanent multipole interactions, provide the dominant intermolecular binding mechanism in molecular solids [9]. Consequently, organic materials are often sublimed and/or solution-processed at lower temperatures relative to their inorganic counterparts, and demonstrate enhanced mechanical flexibility [10, 11]. However, the stronger intermolecular electron coupling that exists within inorganic materials contribute to the formation of physically robust structures that facilitate superior thermal stability and significantly higher charge carrier mobilities [5]. Hence, it is evident that the development of next-generation inexpensive flexible electronics demands unconventional hole-transport materials, which combine the typical advantages of both organic and inorganic solids. The necessity to process such semiconductors over large-area substrates at low cost imposes an additional constraint for the widespread adoption of the technology.

At present, transparent p-type inorganic semiconductor research primarily focuses on two classes of compounds: metal oxides and chalcogenides. Metal oxides are considered the more viable option for industrial applications due to the availability of a range of electron-transporting (n-type) materials. TFTs are often used as test-beds in which the critical parameters of the semiconductor, e.g. field-effect carrier mobilities, are evaluated. Reports of field-effect hole mobilities greater than 5 $cm^2 V^{-1} s^{-1}$ are exceptionally rare, and are only observed in devices that utilize the highest performing transparent p-type oxides [12]. Meanwhile, it is not uncommon for TFTs based on n-type oxide materials with similar properties to achieve electron mobilities that exceed this value by an order of magnitude [13]. There is an increasing interest in high mobility copper compounds, such as copper(I) oxide (Cu_2O), due to their high p-type conductivity, with some reports of field-effect mobilities greater than 1 $cm^2 V^{-1} s^{-1}$ [14–17]. However, p-type oxides, including Cu_2O, pose several disadvantages. Oxides, particularly those of copper, are typically low band-gap materials with limited optical transparency; the 2.1 eV band-gap of Cu_2O is one such example [14]. Furthermore, the deposition of p-type oxide thin-films with optimized carrier-transport properties often necessitates elevated temperatures in excess of 200 °C [16, 17], or relatively expensive deposition processes like magnetron sputtering [15], both of which are unsuitable for application in large-area plastic electronics where low-temperature solution-processing is preferred. Hence, copper(I) thiocyanate (CuSCN), a molecular inorganic semiconductor and its derivatives, offer a promising solution to this rather critical technological challenge.

2. Copper(I) thiocyanate

CuSCN is a molecular, metal pseudohalide of singly-ionized copper, the properties of which have been studied since the first half of the twentieth century [18]. Pseudohalides are polyatomic groups that incorporate a pseudohalogen anion such as thiocyanate and are described as such because they behave similarly to halide ions in chemical reactions. CuSCN is an inexpensive and commercially available material, supplied to laboratories by large-scale international distributors. Readers should note that another copper thiocyanate compound also exists: $Cu(SCN)_2$. While the latter was the subject of several early experiments on pseudohalides [19–22], it is beyond the scope of this review.

2.1. Structural properties of CuSCN

Depending on the preparation procedure, CuSCN precipitated from solution can exist in two forms, its α- and β-phases, which specify structural parameters such as bond angles [23]. The α-phase has an orthorhombic crystal lattice, while the β-phase can be a hexagonal or rhombohedral structure [24]. Although some studies suggest that polymorphic systems containing both phases may be observed, thin-films commonly exhibit the β-phase [25]. CuSCN is an intrinsic semiconductor, which can exhibit p-type conductivity if the solid is formed in a solution where the concentration of thiocyanate ions is higher than that of copper ions [26]. This condition creates a stoichiometric deficiency of copper atoms in the solid, and the hole-transporting character in p-CuSCN is attributed to copper vacancies in the crystal lattice, with acceptor impurity levels generated close to the valence band maximum. Furthermore, the copper defect structure contributes to its optical transparency, because the removal of copper atoms from the perfect crystal lattice broadens the optical bandgap [27]. Conversely, a stoichiometric excess of copper atoms has the opposite effect and facilitates greater n-type conductivity. Moreover, CuSCN demonstrates excellent thermal stability since decomposition of the material into copper sulphide is only observed at temperatures above 300 °C [28, 29].

2.2. Optical properties of CuSCN

Figure 1 shows the transmission and absorption spectra of a solution processed thin-film of CuSCN from which the optical bandgap energies can be determined [30]. In particular, the bandgap values are obtained from plots of $(\alpha h\nu)^n$, where α is the absorption coefficient, h is Planck's constant, and ν is the frequency of radiation; n has a value of 2 for direct bandgap semiconductors, and 1/2 if the bandgap is assumed to be indirect. Thus two different energies, 3.87 eV (direct) and 3.49 eV (indirect), are derived. While the spectral information does not allow one to identify the nature of the bandgap, the values compare well with those from previous studies. For instance, Jaffe *et al* predicted the existence of an indirect bandgap of 3.5 eV from an electronic band structure model calculated using density functional theory, although

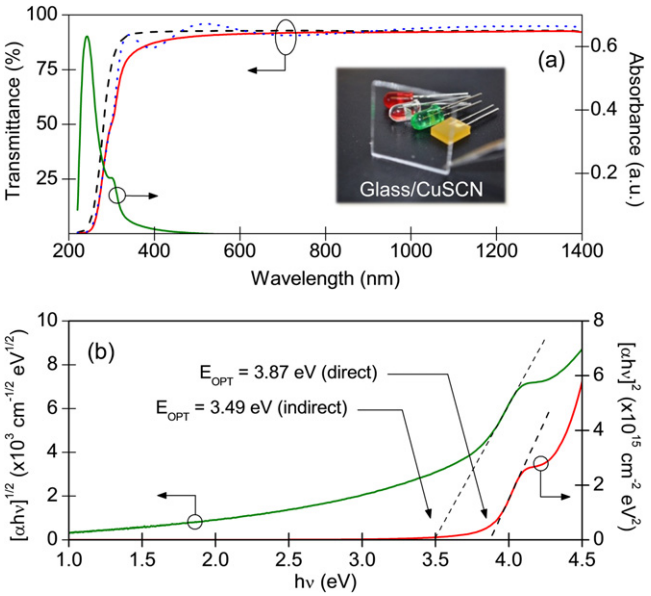

Figure 1. (a) Transmission and absorption spectra from a thin-film of CuSCN on a glass substrate, in its pure form and in a bilayer with a high-k dielectric polymer used in thin-film transistor applications: poly(vinylidene fluoride-trifluoro-ethylene chloro-fluoro-ethylene) (P(VDF-TrFE-CFE)). Inset: photograph demonstrating the high optical transparency of a CuSCN film on glass. (b) Respective direct and indirect bandgap energies of 3.87 and 3.49 eV, corresponding to the marked linear regions, are extracted from plots of $(\alpha h\nu)^2$ and $(\alpha h\nu)^{1/2}$ calculated from the absorption spectrum. Adapted and reprinted with permission from [30], copyright 2013 WILEY-VCH Verlag GmbH & Co. KGaA, Weinheim.

absorption measurements performed on CuSCN samples indicated the presence of an indirect bandgap of 3.9 eV [24]. To this end, energies ranging from 3.6 to 3.94 eV are often quoted in the literature for various films deposited and characterized by different methods, but data to conclusively determine the nature of the bandgap remains inadequate [26, 31–33]. Nevertheless, most reported bandgap values greatly exceed photon energies corresponding to the visible spectral region, indicating that CuSCN is highly optically transparent. Absorption measurements, referenced to glass, show that CuSCN has a remarkable average transparency of 98% in the 390–750 nm optical spectral region [30], and an average transparency of 89% in the 400–1300 nm region [34]. Furthermore, regardless of its exact nature, it is evident that the bandgap in CuSCN is significantly larger than that of commonly used p-type semiconductors such as Cu_2O (~2.1–2.6 eV) [14, 35].

2.3. Hole-transport in CuSCN

Although stoichiometric CuSCN is known to be an intrinsic hole-transporting semiconductor, extrinsic p-type conductivity at room temperature has been observed and was attributed to the formation of acceptor impurity levels close to the valence band maximum due to the presence of copper vacancies in the crystal lattice [26]. Recently, a field-effect hole mobility value of up to 0.1 $cm^2 V^{-1} s^{-1}$ was reported for TFTs based on solution-processed nanocrystalline CuSCN

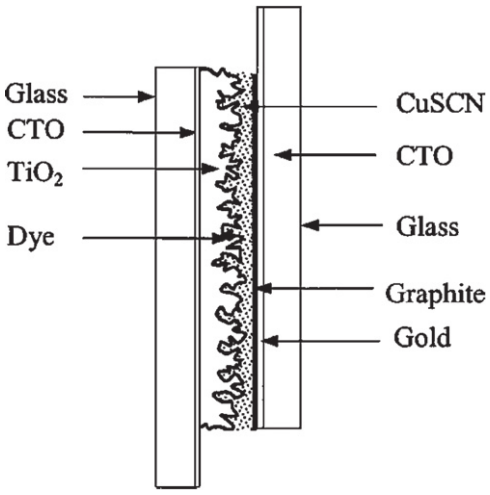

Figure 2. Schematic of a dye-sensitized NIR photodetector with n-TiO_2; p-CuSCN is used as the hole conductor. Reprinted with permission from [36], copyright 2004 AIP Publishing LLC.

films [25, 30]. It was shown that devices prepared and tested in inert atmosphere exhibit intrinsic hole-transporting characteristics but a significant p-type like doping effect was observed upon exposure of the transistors to air for a few days. In addition to extrinsic doping effects, the hole-transport characteristics of CuSCN are also known to be strongly dependent on fabrication conditions as well as device geometry, electrode contact resistance and dielectric/semiconductor interface trap density [30]. However, the underlying physical mechanisms are yet to be investigated and understood and further work would be required. This work strongly suggests that while the maximum reported hole mobility in CuSCN falls below that of the best performing p-type semiconductors at present, optimization of fabrication parameters could, theoretically, produce a dramatic improvement in hole-transport properties of thin-films of CuSCN.

2.4. Applications of CuSCN

Early research on CuSCN explored its photocatalytic properties [37], as well as its use in generation of dye-sensitized photocurrents [38]. While the electronic band structure of p-CuSCN limits its suitability as a photocathode, the adsorption of dye molecules at the semiconductor surface modifies the spectral response of the composite system and amplifies photoresponsivity. However, dye-sensitized n-type titanium dioxide (n-TiO_2) shows far superior photocatalytic properties, and nanostructured n-TiO_2 films soon became a central component of many dye-sensitized systems. The schematic diagram in figure 2 is an example of a low-cost, near infra-red (NIR) photon detector [36]; the p–n heterojunction contains p-CuSCN and n-TiO_2, deposited onto a glass substrate with a conductive-tin-oxide (CTO) coating, where the gold-plated CTO-glass substrate on the opposite side functions as the back contact. Following photoexcitation, dye molecules at the semiconductor interface inject holes into the valence band of p-CuSCN and electrons into the

conduction band of n-TiO_2 to generate a measurable photocurrent. The roughness of the dye-sensitized TiO_2 film creates a large surface area for light absorption.

Flexible substrates can be used as an alternative, and the peak spectral response of the device can be tuned by modifying the chemical structure of the dye. However, further research is required to optimize device responsivity and response time to compete with similar NIR detector technologies; the slow diffusive transport of electrons in TiO_2 films is a particular hindrance. In contrast, rapid 4 ns response times are observed in ultra-violet (UV) photodetectors that incorporate CuSCN and zinc oxide (ZnO) nanorod heterojunctions [40]. The heterojunction is photoactive without dye-sensitization: as wide-bandgap semiconductors, CuSCN and ZnO show high transparency in the visible spectral region, but readily absorb higher energy photons of UV frequencies. More recent studies on the UV photoresponse properties of CuSCN and ZnO-nanorod heterojunctions have also yielded promising results and further demonstrated the potential to develop self-powered UV photodetectors with rapid response times [41, 42], where the device selectivity can be modulated by controlling the length of ZnO-nanorods [42]. Other dye-sensitized systems containing CuSCN are found in photoelectrochemical cells [43–47], with CuSCN-based dye-sensitized heterojunctions for photovoltaic cells soon proposed and realized by O'Regan and Schwartz [48–50].

The processing versatility of CuSCN allows it to be integrated into various types of p–n heterojunctions, where TiO_2 [39, 51] or ZnO [52–57] are typically used as the n-type semiconductor. Figure 3 shows an example of the diode-like rectifying behaviour of a simple p-CuSCN and n-TiO_2 heterojunction, and a scanning electron microscope (SEM) image of the porous TiO_2 surface, with maximized contact area, into which CuSCN is filled using an electrochemical method. Despite the simplicity and low-cost of this solution-based fabrication process, the resulting devices were found to exhibit excellent electrical contact and rectification. However, a more complicated pulsed deposition process was shown to significantly improve the device performance [55]. Other electronic devices that incorporate CuSCN into heterostructures include spray-deposited p–n junction diodes [58], flexible hybrid diodes embedded into polymer matrices [59], solar cells with ZnO-nanorod arrays [60], and ZnO-nanorod based light-emitting diodes (LEDs) shown in figure 4 [61]. Enhanced emission is observed in the visible spectral region due to an increase in surface states and defects at the ZnO surface, which is induced by the electrochemical growth of the CuSCN layer. Using CuSCN as the hole-transport material was also found to balance the carrier injection rates, which in turn increases the efficiency of radiative recombination and hence the overall LED efficiency.

Research on the charge transport and dye-sensitization of CuSCN and its use in p–n heterojunctions provided the foundation for investigations into three key application areas relevant to the development of next-generation large-area electronics: (i) TFTs, (ii) photovoltaic cells (organic and hybrid organic-inorganic), and (iii) OLEDs. The remainder of this review article provides a comprehensive discussion on the fabrication and characterization of such devices.

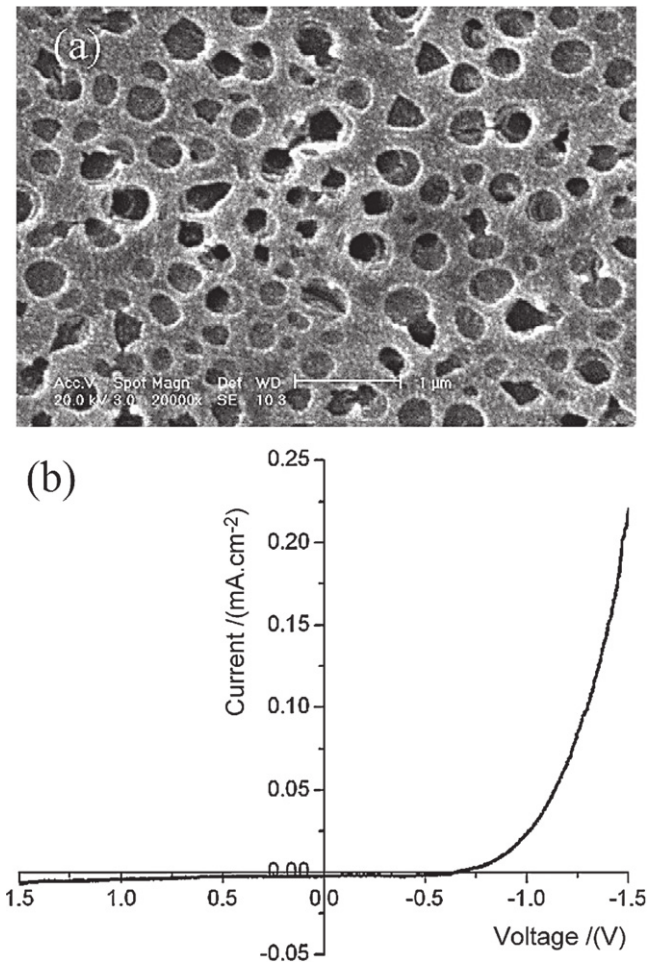

Figure 3. (a) An SEM image of the as-prepared porous n-TiO_2 surface into which p-CuSCN is filled to form a heterostructure. (b) Current–voltage characteristic of the corresponding p–n heterojunction. Adapted and reprinted from [39], copyright 2007 with permission from Elsevier.

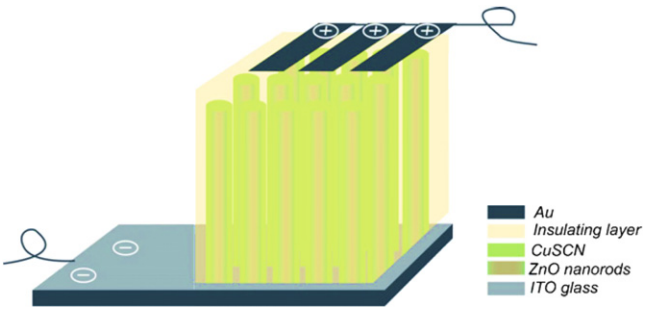

Figure 4. Schematic of an LED with a n-ZnO nanorod and p-CuSCN heterojunction; a gold (Au) cathode and an ITO anode is used. Reprinted from [61], copyright 2007 with permission from Elsevier.

3. Deposition of CuSCN

Fabrication of large-area plastic electronics requires semiconductor deposition techniques that minimize device

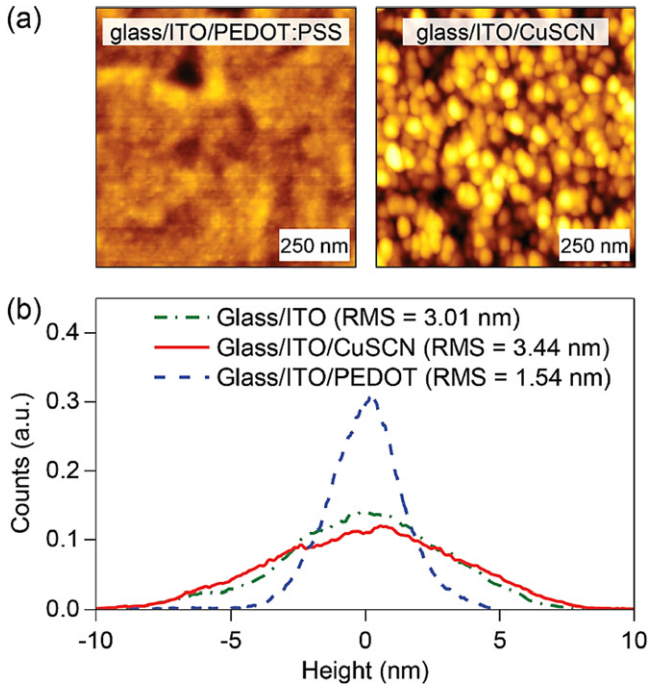

Figure 5. (a) AFM images of PEDOT:PSS (left) and CuSCN (right) films spin-coated onto ITO-coated glass substrates. (b) Histogram showing surface height distributions calculated from the AFM topography measurements. Adapted and reprinted with permission from [34], copyright 2014 WILEY-VCH Verlag GmbH & Co. KGaA, Weinheim.

production costs and avoid thermal degradation of temperature-sensitive active materials. Hence, all techniques utilized must involve low temperature and cost-efficient processes ideally performed at atmospheric pressure. A variety of methods, ranging from spray-coating [54, 58], to successive ionic layer adsorption and reaction (SILAR) [33], have so far been implemented for the fabrication of CuSCN hole-transport layers (HTLs). However, in-depth analysis of each procedure is beyond the scope of this review. Therefore, in this section, we introduce and focus on three techniques commonly used for large-area deposition of CuSCN, and evaluate the results reported thus far.

3.1. Spin-coating

The deposition of CuSCN films via spin-coating is frequently reported in the literature [24, 25, 30, 34, 62, 63]; one such example is presented in figure 5(a). Parameters that control film thickness include the concentration of the solution, its viscosity, and the angular speed of rotation. Despite its simplicity, this method presents some challenges. For example, high solubility of CuSCN in a solvent suited to low-temperature processing is required. Furthermore, the material solution must exhibit solvent orthogonality such that it does not react with other device components. Due to the significant quantity of material discarded during the spin-coating process, it is also essential that a low-cost solvent is used.

Following the identification of n-propyl sulphides as appropriate solvents for the formation of stable CuSCN solutions at room temperature [64], spin-coated films, annealed at 70–80 °C, were produced using dipropyl sulphide (DPS) [24]. Unfortunately, CuSCN has limited solubility in DPS rendering deposition of thicker films via spin casting highly problematic. Conversely, diethyl sulphide (DES) readily produces non-saturated solutions at appreciable concentrations in the range of 10–40 mg ml^{-1}. This enhanced solubility was found to dramatically improve the continuity and uniformity of deposited films, hence allowing for superior control over the thickness of HTLs [34]. Organic photovoltaic cells and OLEDs that contain spin-coated CuSCN interlayers are thus produced [34, 63], in addition to TFTs and unipolar logic circuits [30]. AFM topography measurements in figure 5(a) show a comparison of 45 nm thick films formed using CuSCN, and the common HTL material, poly(3, 4-ethylene dioxythiophene) polystyrene sulphonate (PEDOT:PSS), spin-coated onto ITO-coated glass. Surface height distributions calculated from the topography data are given in figure 5(b). The HTL materials are deposited onto ITO-coated glass for solar cell applications because ITO is a transparent conductor. While both CuSCN and PEDOT:PSS films exhibit high uniformity, further optimization is required to improve the quality of the CuSCN film relative to PEDOT:PSS. Finally, spin-coating is also suited to deposition of CuSCN-nanorods from o-dichlorobenzene solutions. These nanorods have been reported to form scaffolds in bulk heterojunction (BHJ) solar cells and improve charge-carrier collection [62].

3.2. Printing methods

Following the success of drop-cast deposition procedures [64, 66], several reports of inkjet-printed CuSCN HTLs emerged [67–69]. It was shown that the morphology of the inkjet-printed CuSCN dependents on deposition temperature and the properties of the ink, and hence, device performance varies accordingly. Although very promising, the method requires significant optimization because inkjet-printing of CuSCN often leads to the formation of large discontinuities in the film, which in turn results in poor device performance [68]. Applying CuSCN solution using the wiping process (figure 6), was shown to produce HTLs of superior quality relative to inkjet-printed layers [65, 70]. Low-cost, volatile solvents, such as DPS, are well suited to both the wiping and inkjet-printing methods.

It is also possible to use doctor-blade processes to produce CuSCN HTLs for large-area printed electronics, with printed hybrid perovskite solar cells (PSCs) being one such example [71]. It has been shown that the inclusion of printed CuSCN HTLs significantly increase the photocurrents generated. The effect was attributed to the improved charge separation originating from the excellent hole-extraction properties of CuSCN. Direct comparisons with alternative deposition methods are not available in the literature.

3.3. Electrochemical deposition

In addition to the aforementioned research on p–n heterojunctions, numerous other studies succeeded in using

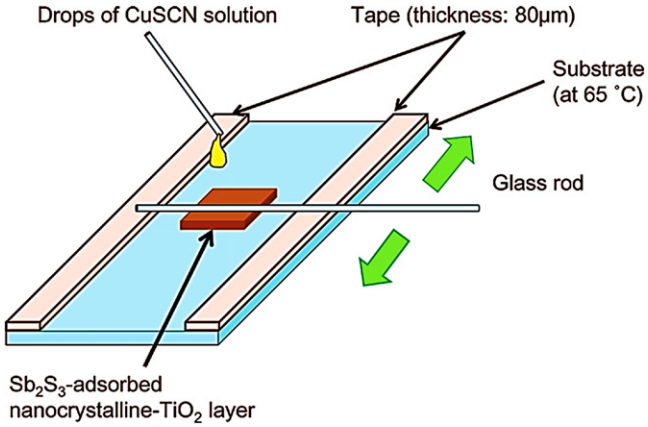

Figure 6. Schematic of a wipe-deposition process suited to the application of CuSCN HTL in solar cells. Antimony trisulphide (Sb_2S_3) is the photon absorbing material, while TiO_2 forms the electron-transport layer. Reprinted with permission from [65], copyright 2012 American Chemical Society.

electrochemical deposition methods to produce CuSCN HTLs [73–77]. Paunovic and Schlesinger have explained the fundamentals of this rather interesting low-temperature, solution-based deposition technique [78]. In brief, an aqueous solution of potassium thiocyanate (KSCN) is generally used as the electrolyte for deposition of CuSCN. The electrolyte contains constituent charged ions of CuSCN, which form a semiconductor film on an immersed electrode when the solution is electrolysed. The morphology of electrochemically grown films is found to be dependent on several growth parameters, which include deposition time, applied potential and ion concentration. Fabrication temperatures and financial costs are minimized because post-deposition thermal annealing is often not a requirement, although a slight increase in the optical band-gap was observed following high temperature annealing [79]. However, the necessity to deposit the semiconductor onto a conductive surface limits the applicability of this method. For instance, it is not suitable for fabrication of TFTs, where CuSCN is typically deposited onto a dielectric. This limitation can be better understood from the device architectures illustrated in figure 7 where the semiconductor is always deposited onto the surface of a dielectric or on the top of an insulating substrate.

Heterojunctions containing electrodeposited CuSCN exhibit good rectification characteristics [39], while electrodeposited layers of CuSCN playing the role of HTLs in organic and PSCs have yielded promising results [80, 81]. Moreover, addition of chelating agents to CuSCN solutions was found to yield nanorod arrays of high crystallinity [81–83]. In these studies, the nanorod diameter and density was found to depend on the thiocyanate ion concentration and the applied electrical potential. This fabrication method is thus promising for the formation of nanostructured optoelectronics, while the low temperature requirements make it ideal for deposition of CuSCN onto inexpensive flexible substrates [83].

4. Thin-film transistors

The commercial success of optical display technologies that utilize electron-transporting TFTs based on transparent n-type oxide semiconductors have stimulated significant research focusing on development of complementary p-type material technologies with similar performance characteristics [5–7, 84]. Furthermore, hole and electron-transporting TFTs are both key components of the highly successful complementary logic circuitry—also known as metal-oxide-semiconductor (CMOS) technology—often used to fabricate large scale integrated circuits (inorganic as well as organic) with high yield [85, 86]. Finally, TFTs also provide a unique test-bed in which the electronic properties of a given semiconductor can be evaluated and the deposition parameters can be carefully optimized prior to incorporating the active material into opto/electronic devices and systems with more complex architectures.

A standard TFT has three terminals: the source (S), drain (D) and gate (G) contacts. Device architectures are classified according to the relative positions of the terminals, few of which are displayed in figure 7. Associated advantages and disadvantages depend on the materials used and not the device configuration alone. The charge transport model that is commonly used for the analysis of standard TFTs is governed by the gradual channel approximation [87], but a detailed mathematical treatment of the operating principles is beyond the scope of this review. Instead, the primary aim of this section is to provide a qualitative description of the basic operating principles and at the same time summarize recent developments in the area of solution-processed p-channel CuSCN-based transistors.

4.1. Operating principles of TFTs

In hole-transporting TFTs, modulation of a positive channel current flowing between the metallic S and D terminals by the applied gate field (V_G) forms the basis of the device operation. As can be seen in figure 7, the gate electrode is always separated from the semiconductor by the gate dielectric and the source terminal is grounded such that it corresponds to zero potential ($V_S = 0$ V). Electrode materials with appropriate work-functions (i.e. matching energies) are selected to optimize hole-injection and reduce parasitic effects such as large contact resistance (R_C). Application of an external electric field via the gate electrode, in the form of a gate voltage (V_G), modulates the conductivity of the semiconductor region in proximity to the gate dielectric. When a source-drain voltage (V_D) is applied to the device, injected charge carriers (holes and electrons for p-channel and n-channel devices, respectively) accumulate at the semiconductor-insulator interface giving rise to a channel current that flows between the S and D terminals. When the electric field strength corresponding to V_D is significantly smaller than that of V_G, the TFT operates in the so-called linear regime: the distribution of holes across the channel is uniform and the channel current (I_D) depends linearly on the applied S–D field i.e. V_D. If the field strengths corresponding to V_G and V_D are comparable, the device enters

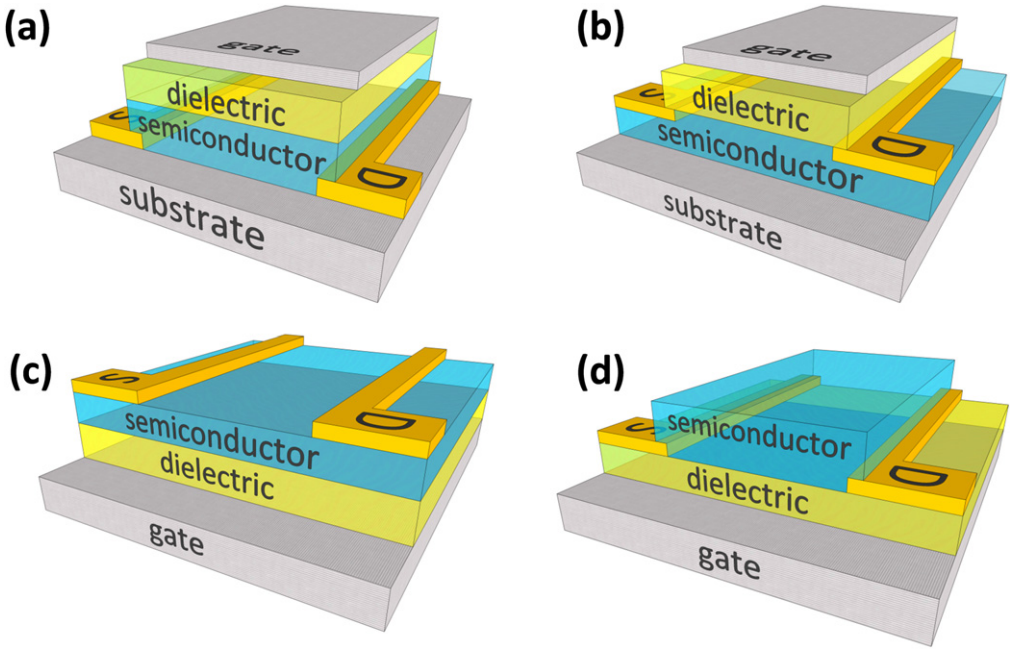

Figure 7. Schematic of TFT architectures. (a) Staggered, top-gate; (b) coplanar, top-gate; (c) staggered, bottom-gate; and, (d) coplanar, bottom-gate. Reproduced from [72] with permission of The Royal Society of Chemistry.

the saturation regime, where I_D saturates and becomes independent of V_D. This is the point at which the depletion of holes occurs at the region closest to the drain electrode, and thus the channel is described as pinched-off. The two regimes can be observed experimentally from the output characteristics of the device.

AFM images in figure 8(a) show the homogenous and highly nanocrystalline structure of a transparent CuSCN film of 45 nm thickness, spin-coated onto plain glass from a DES solution, for the purpose of TFT fabrication. Several important performance-related parameters can be extracted from the transfer characteristics (figure 8(b)) of a TFT [34]. One key parameter is the threshold voltage (V_{TH}), which quantifies an offset in the hole distribution that contributes to hole-transport in the absence of a gate potential. This offset can originate from multiple sources, including, charge-carrier trapping in the bulk semiconductor, or interface trap-state formation at the semiconductor-insulator boundary [88]. Another such variable is the on-to-off channel current ratio, which defines the difference between maximum I_D measured in the on-state, and the leakage current that often dominates the channel's off-state. This value is usually specified in orders of magnitude and a low ratio is indicative of poor switching functionality. Most importantly, the field-effect hole mobility for both linear and saturation regimes can easily be computed directly from the transfer characteristics (figure 8(b)) using the aforementioned transistor model [72].

4.2. CuSCN TFTs

Hole-transporting TFTs based on p-CuSCN are a recent development [25, 30, 34]. In these devices the semiconductor films are deposited from solution in DPS or DES at room-temperature via spin-coating. The method is simple and highly scalable, while it enables use of inexpensive and temperature sensitive substrate materials such as plastic. In these early reports it has been shown that the device performance depends heavily on the device configuration and particularly on the position of the S–D electrodes. Two types of device architectures have so far been demonstrated, namely, the coplanar bottom-gate structures, and the staggered top-gate structures. The latter have shown superior performance as compared to coplanar TFTs. This is partly explained by a difference in architecture-related parasitic contact effects since discontinuities in hole concentration can result from irregularities in the channel potential profile, which in turn limits carrier injection and increases parasitic contact resistance R_C [89, 90].

The transfer characteristics for a staggered top-gate TFT is shown in figure 8(b) [34]. Low hysteresis is primarily attributed to a high-quality semiconductor-insulator interface [30], while the high on/off channel current ratio is indicative of the intrinsic semiconducting nature of the solution-processed CuSCN layer. Field-effect hole mobilities up to 0.1 $cm^2 V^{-1} s^{-1}$ were observed in TFTs that incorporate the high-k relaxor ferroelectric polymer dielectric P(VDF-TrFE-VFE). While parasitic contact resistance and interface charge-traps are both factors that limit carrier mobility [91], the combined effects in CuSCN TFTs are yet to be fully understood. Roughness of the film surface is suspected as the origin of relatively high trap concentrations present in the P(VDF-TrFE-VFE) layer. While TFTs with the transparent amorphous fluoropolymer, Cytop, as the dielectric exhibit good hole-transport properties, using a high-k material has the added advantage of producing devices that operate at significantly lower voltages and as such consume less power. The hole mobilities in comparable p-type semiconductor

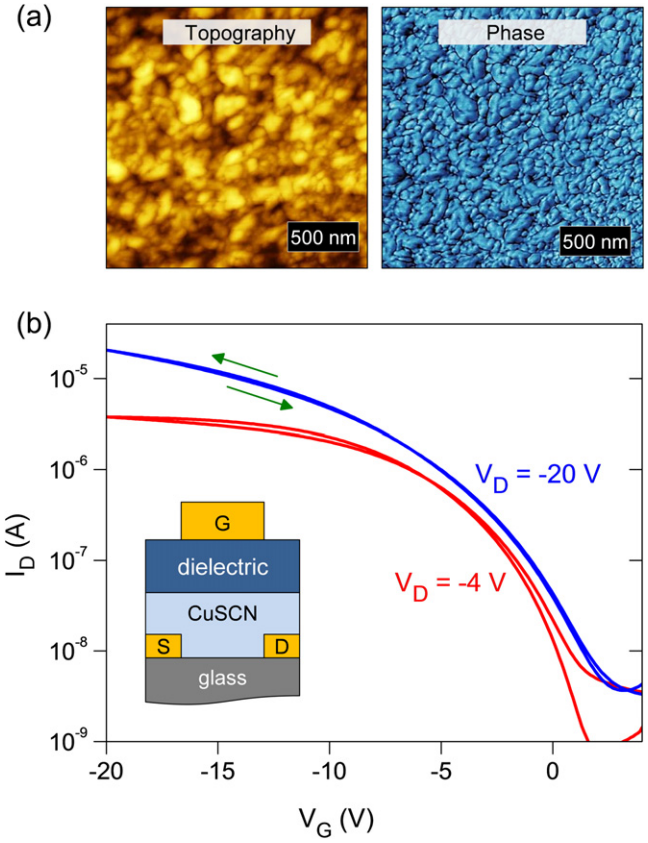

Figure 8. (a) AFM surface topography (left) and phase (right) images of a 45 nm thick CuSCN film deposited onto a glass substrate. (b) Transfer characteristic data from a CuSCN TFT, with 30 μm channel length and 1 mm channel width. Inset: schematic of the TFT architecture, illustrating thin-films deposited onto a glass substrate. Source and drain contacts are gold; the gate contact is aluminium. The dielectric used in this instance is the high-k polymer, P(VDF-TrFE-CFE). Reprinted with permission from [34], copyright 2014 WILEY-VCH Verlag GmbH & Co. KGaA, Weinheim.

technologies, such as copper oxide TFTs, rarely exceed unity [5]. Therefore, while further optimization of fabrication processes is required in order to compete with the highest performing p-type TFTs, the results from CuSCN transistors are encouraging thus far.

Finally, good distribution in performance parameters, such as V_{TH} (−2 to −3 V) and on-to-off channel current ratio (10^4), have been reported for CuSCN TFTs, further demonstrating the potential of the material. This excellent device reproducibility and low operating voltages, have allowed integration of CuSCN TFTs into functioning logic gates such as voltage inverters (i.e. NOT gates). The latter type of circuits have been shown to exhibit voltage signal gain of >2, with appreciable noise margins, which make them interesting for future microelectronic applications [30].

5. Photovoltaic cells

There is an immense interest in OPV [10, 11, 92–97] and hybrid organic-inorganic photovoltaics [4, 98–101] for large-area applications. Such devices offer low-cost, flexible alternatives to traditional silicon technologies, while at the same time promise a significant expansion of the application space far beyond what is currently covered by incumbent technologies.

Unfortunately, these emerging technologies often exhibit inferior power conversion efficiencies (PCE) relative to inorganic devices. The latter disadvantage is primarily attributed to the low charge-carrier mobility, and inferior solar spectral absorption and charge dissociation characteristics in most organic semiconductors [103, 104]. However, tremendous progress has been made in high-efficiency OPV and hybrid cell research, with reports of PCE approaching and surpassing 10% [105, 106]. It is therefore essential to identify methods to further increase the PCE in order to compete with existing inorganic technologies, and the use of alternative HTLs can be seen as a promising step towards this direction. Based on the physical characteristics of CuSCN discussed so far, it can be argued that it may be an ideal HTL candidate. For example, it exhibits excellent hole-transport characteristics, is highly transparent in the optical spectral region, and is solution-processable at low temperature. Furthermore, and unlike semi-metallic HTL materials such as PEDOT:PSS, CuSCN is an intrinsic semiconductor and as such facilitates excellent electron blocking which can help to minimize exciton recombination at the anode side. Because of its attractive properties CuSCN has been used as a transparent hole conductor in solid-state inorganic photovoltaic cells for more than a decade [68, 107–109], including cells that employ an extremely thin absorber (ETA) [110–115], as well as in quantum dots-based devices [116, 117]. With the exception of dye-sensitized solar cells (DSSCs), reports of organic and hybrid photovoltaic cells with CuSCN remained limited despite their potential, until recent years. This section provides a simplified description of photovoltaic cell operation and discusses new developments in research on CuSCN HTLs for organic and hybrid photovoltaics.

5.1. Operating principles of organic/hybrid BHJ solar cells

Efficient organic and hybrid photovoltaic cells can be manufactured utilizing the BHJ concept [118–120] illustrated in figure 9 [102]. In the standard geometry, photons enter the cell through a transparent anode electrode and reach the BHJ active layer, which is typically a nanostructured composite of two materials, the so-called donor and an acceptor. Donors are often semiconducting organic polymers; they function as primary absorbers that transfer excited electrons to the acceptor materials (inorganic system or an organic semiconductor). The BHJ concept offers ambipolar charge transport and excellent internal quantum efficiencies because energy bands in the constituent materials are tuned to optimize photon absorption and photo-generated charge transport and collection [119]. Photons with energies that exceed the bandgap are absorbed, leading to electron-hole pair (exciton) generation. Excitons diffuse through the BHJ, and separate into electrons and holes at the extended donor-acceptor interfaces. The separated charge-carriers drift and diffuse

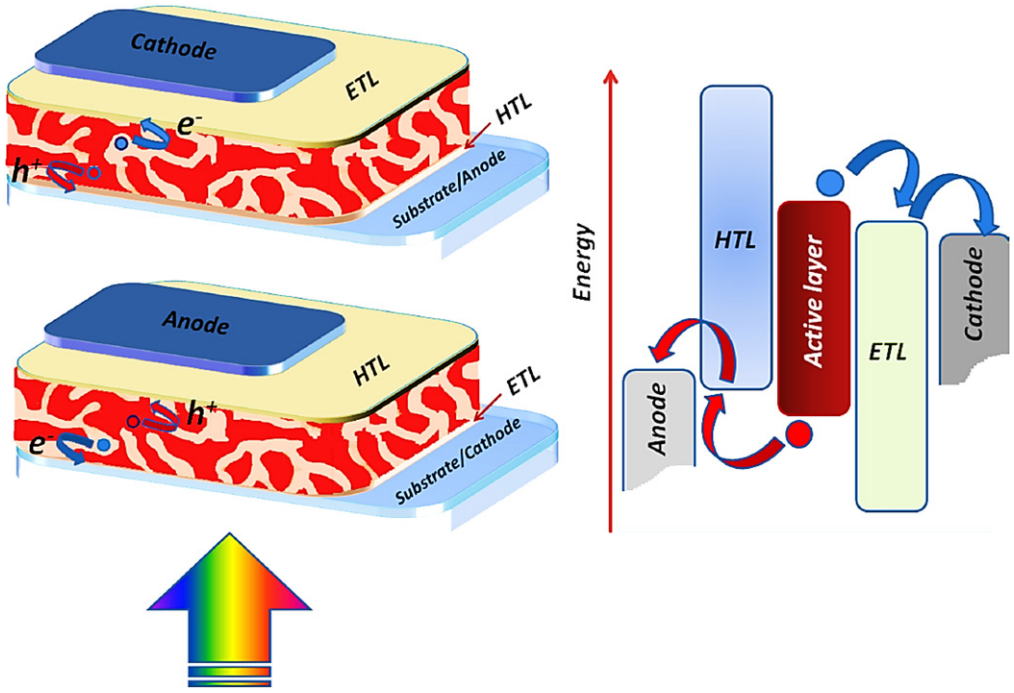

Figure 9. Schematic of standard (top) and inverted (bottom) geometries for a BHJ photovoltaic cell, accompanied by an energy level diagram of the constituent layers. The arrow below the schematic represents the direction of incident photons; blue circles represent electrons and red circles represent holes. Reprinted from [102].

through to the HTL and the electron-transport layer (ETL), after which they are transported into an external circuit via the electrodes to generate a photocurrent. Figure 9 shows that the standard cell geometry demands HTLs with high optical transparency to minimize absorption of incident photons because the solar emission spectrum peaks at visible frequencies. Furthermore, device performance is optimized if the HTL exhibits good electron-blocking properties and stops electrons from reaching the anode. Additionally, inverted geometries can be used if the oxidation of the low work-function cathode in ambient air conditions presents a problem [102].

Typically, photovoltaic cells are characterized by measuring their current–voltage (*I–V*) characteristics under simulated air mass 1.5 global (AM1.5G, 1 Sun) irradiation using a solar simulator, and in the dark. PCE is thus the measure of maximum electrical output power relative to total incident optical power. Another parameter extracted from *I–V* curves is the fill-factor (FF), which defines output at the maximum power point relative to the potential power. Meanwhile, short-circuit current density (J_{SC}) is the per unit area photocurrent under AM1.5G illumination with zero applied bias, and open-circuit voltage (V_{OC}) is the applied voltage at which the photocurrent is zero. The spectral dependence of photocurrent is also measured. This gives another measure of efficiency, described as incident-photon to collected-electron (IPCE), or external quantum efficiency (EQE).

5.2. Organic BHJ photovoltaic cells

In general, OPV cells are devices that contain an organic active layer. BHJ OPV cells often contain an active layer with an interpenetrating polymer:fullerene blend. A conjugated polymer, such as poly(3-hexylthiophene-2, 5-diyl) (P3HT), typically serves as the light absorber. Common soluble acceptors include the fullerene derivative, phenyl-C61-butyric acid methyl ester (PCBM). Upon photon absorption, electrons are excited from the highest occupied molecular orbital (HOMO) of P3HT to its lowest unoccupied molecular orbital (LUMO), and then relax to form excitons. In the ideal case, the formed excitons diffuse and dissociated at the critical donor:acceptor interface with the free electron transferred to PCBM, and eventually to the cathode electrode, while the hole is transferred via the donor polymer to the anode electrode. The traditional hole-transporting/extracting layer in standard polymer: fullerene devices is poly(3, 4-ethylenedioxythiophene) doped with polystyrenesulphonate (PEDOT:PSS). However, its use as an interlayer causes instabilities due to its acidic nature because it can chemically react with the active layer [121], or etch the ITO anode [122]. This rather critical technology bottleneck has prompted a significant search for unconventional HTLs that improve both device lifetime and PCE.

Recently Yaacobi-Gross *et al* have reported the use of CuSCN as a promising HTL in high efficiency organic BHJ cells (figure 10) and compared the cells' performance against control cells made using PEDOT:PSS [34]. It was shown that nanocrystalline films of CuSCN, spin-coated from solution in DES with controlled thickness, show greater transparency in visible and NIR spectral regions relative to PEDOT:PSS films with similar thickness. Although CuSCN films were found to exhibit lower uniformity across the substrate, the resulting devices produce similar open circuit voltage (V_{OC}) and FF with PEDOT:PSS devices, but significantly higher short

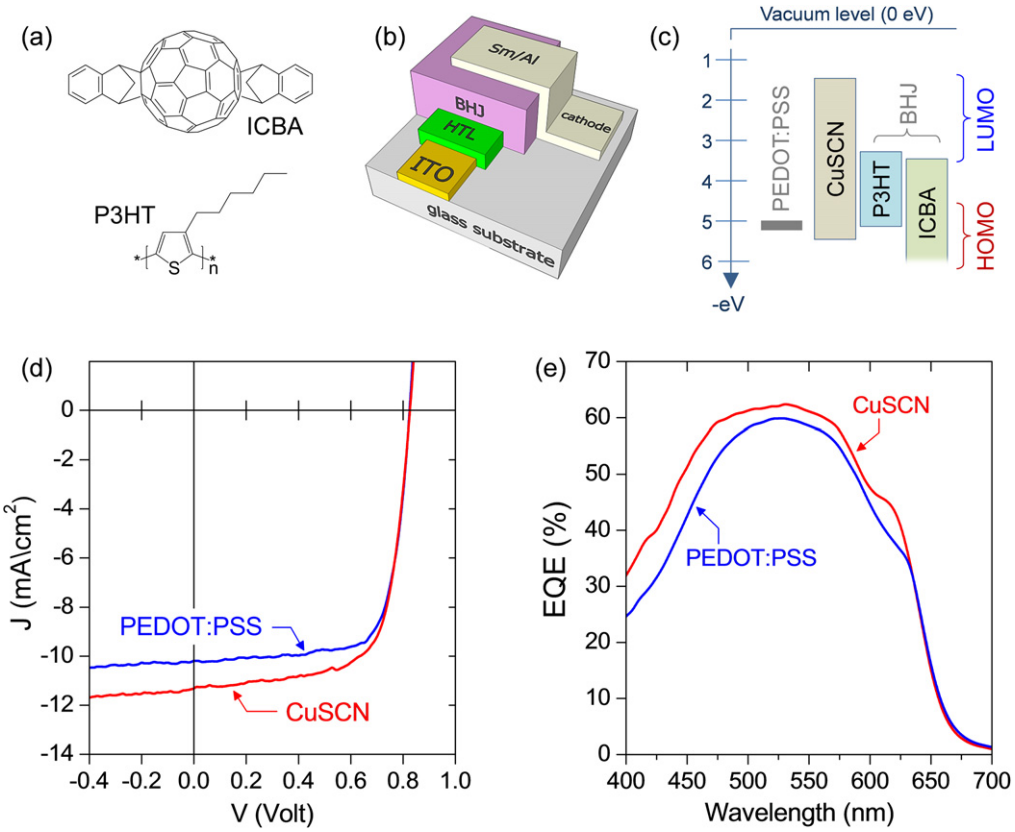

Figure 10. (a) Molecular structure of P3HT and ICBA. (b) Schematic of the BHJ OPV cell, with a transparent ITO anode and a samarium/aluminium (Sm/Al) cathode. (c) Energy level diagram of the constituent materials. (d) Comparison of current density–voltage (*J–V*) characteristics for P3HT:ICBA cells with CuSCN and PEDOT:PSS HTLs, under AM1.5G illumination. (e) Corresponding EQE spectra from P3HT:ICBA cells. Reprinted with permission from [34], copyright 2014 WILEY-VCH Verlag GmbH & Co. KGaA, Weinheim.

circuit current (J_{SC}). Consequently, cells with CuSCN as HTLs produce superior PCE of 6.2%, and EQE that is approximately 5% higher than PEDOT:PSS-based devices due to enhanced transparency of CuSCN across the relevant spectrum. PCE greater than 8% was also reported for some devices containing alternative polymer:fullerene blend combinations [34]. A further key observation was that the valence band position of CuSCN is well suited for use as a HTL and does not hinder the cell's efficiency.

In the case of planar (layered) heterojunction P3HT:PCBM cells incorporating low-temperature electrodeposited CuSCN HTLs, a marginally lower PCE of 2.5% was achieved, relative to devices with PEDOT:PSS (PCE = 2.6%) [123]. It was established that the cell's efficiency strongly depends on deposition parameters of CuSCN such as solution concentration and temperature. Furthermore, electrodeposited CuSCN nanowires (NWs) have shown excellent potential as a novel HTL material for polymer:fullerene BHJ devices [81]. These types of HTLs were tested in OPVs with blends consisting of $PC_{70}BM$, as the acceptor, and poly[N-9′-heptadecanyl-2, 7-carbazole-alt-5, 5-(4′,7′-di-2-thienyl-2′, 1′, 3′-benzothiadiazole)] (PCDTBT) as the donor polymer. Importantly, the lack of a high-temperature annealing step during deposition lowers fabrication costs and facilitates the use of inexpensive plastic substrates. Comparisons with CuSCN thin-films indicate that the nanostructuring provided by CuSCN NWs improves OPV performance by enhancing the hole extraction properties of the HTL, with the PCE value increasing from 3.3 to 5.1% for thin-film and NW HTL devices, respectively. However, both PCE values were found to be lower than that of reference devices made using PEDOT:PSS as the HTL. It was argued that further optimization of the active layer thickness to NW length ratio should lead to improved cell performance. Additionally, in optical modelling considerations for multilayer tandem OPV cells with donor:acceptor as the active layers, CuSCN HTLs were proposed as a superior alternative to PEDOT:PSS HTLs, due to the acidic nature of the latter that tends to damage the frequently used ZnO-based ETLs, allowing for maximum optical absorption [124].

5.3. Hybrid organic-inorganic photovoltaic cells

The term 'hybrid' is often used to describe a broad range of energy generation technologies. In this context, it refers to devices which contain a mixture of organic and inorganic materials in the active layer to profit from the advantages of both. Three primary types of hybrid photovoltaic cells with CuSCN HTLs have so far been reported. These are, (i) the BHJ photovoltaic cells [62], (ii) the organo-metal PSCs [71, 80, 126–129], and (iii) the dye-sensitized solar cells (DSSCs) [64, 66, 130–134].

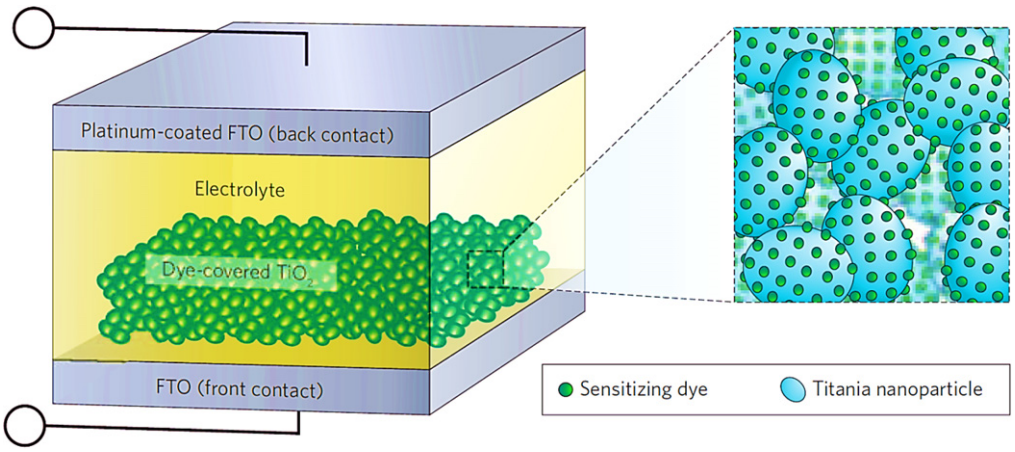

Figure 11. Schematic of the original liquid-based DSSC design. Two FTO-coated glass substrates, including one plated with Pt, form the front and back contacts. The dye-sensitized nanostructured titania (TiO_2) forms the photocathode, and the redox mediating electrolyte facilitates the regeneration of dye molecules following photoexcitation. Adapted by permission from Macmillan Publishers Ltd: Nature Photonics [125], copyright 2012.

The operating principles of hybrid BHJ cells are similar to organic BHJ devices. In the former case, the active layer usually contains an organic semiconducting polymer as the donor, blended with an inorganic semiconducting material (commonly nanoparticles, quantum dots, etc.) acting as the acceptor component. Alternatively, the active layer contains an organic polymer:fullerene blend, with a HTL or ETL material penetrating into the active region in the form of an inorganic nanostructured scaffold that functions as a high-mobility pathway for improved charge-carrier extraction/collection. CuSCN nanorod scaffolds have been successfully implemented in P3HT:PCBM BHJ cells [62]. The observed trends in device performance are similar to cells with ZnO scaffolds, where an inverse proportionality between PCE and nanorod length is observed. However, the inclusion of CuSCN scaffolds lowers both the J_{SC} and FF, and as such the resulting PCE is inferior to devices without scaffolds. Currently, there is insufficient evidence to conclusively determine the origins of poor device performance and further work will be needed.

DSSCs are an extensively studied topic with some reports of PCE exceeding 10% [135–142], and their applicability as large-area flexible devices is an incentive to conduct further research [143]. DSSCs often employ n-type semiconductors as photoelectrodes. Reports of DSSCs with dye-sensitized p-type semiconductors are less frequent due to their inferior PCE [144]. The original liquid-based DSSC design is illustrated in figure 11 [125]. The device was fabricated onto a glass substrate, coated with a transparent conducting oxide, such as fluorine-doped tin oxide (FTO). A monolayer of a dye that exhibits strong absorption of visible light frequencies is covalently bonded to the surface of a nanostructured metal oxide photoanode, usually consisting of mesoporous n-TiO_2. Dye-sensitization of such nanostructured photoanodes amplify photoresponsivity of the device and hence increase the overall device performance. Dye molecules can be purely organic or metal complexes with organic ligands. Upon illumination, photo-excited electrons are transferred from the LUMO of the dye to the conduction band of TiO_2. The back contact (cathode) is typically a conductive substrate with an added catalyst layer, such as platinum (Pt). Presence of a hole-conducting electrolyte mediates redox reactions and facilitates dye-regeneration through charge transfer. However, volatility and leakage risks associated with liquid electrolytes present serious disadvantages, and it is thus beneficial to substitute the liquid electrolytes with solid-state hole-transport materials (HTMs) such as p-CuSCN.

Reports on the use of CuSCN in DSSCs as transparent solid-state HTMs follow from the development of dye-sensitized heterojunctions with CuSCN [48, 49]. The discovery of n-propyl sulphides as orthogonal solvents for solution-based deposition of CuSCN led to the construction of the first functional CuSCN-based solid-state DSSC, with PCE of 1.25% [64]. Nanocrystalline HTMs are deposited from solution in DPS onto substrates heated to 75–85 °C, using a simple drop-casting method, which eliminates the dye degradation problem associated with electrodeposition. However, the suggestion that DES is an unsuitable solvent due to its strong complexation with copper ions, is contradicted by later studies that successfully deposited CuSCN HTLs from solution in DES using similar annealing temperatures [34].

Other studies reported limited success since although the CuSCN was shown to behave as a functional solid-state hole conductor in DSSCs, the resulting cell's PCE remained low and rarely exceeded 2%, i.e. a value significantly inferior to that measured for liquid electrolyte-based devices [66, 130–134]. Conductivity enhancement of the CuSCN HTMs was thus proposed as an option to improve DSSC performance, with several reports on DSSC cells with PCEs >3% [145–148]. Significant increase in the hole conductivity in CuSCN can be achieved using several techniques including: (i) creating a greater stoichiometric excess of SCN^- by exposing CuSCN films to halogen gases or $(SCN)_2$ in organic solvents [145]; (ii) by modifying the CuSCN crystal structure by introducing triethylamine coordinated Cu^+ sites with $(SCN)_2$

contaminants [146], or (iii) by introducing triethylamine coordinated Cu^{2+} sites [147, 148]. However, the resulting device efficiencies were significantly lower than that of the highest-performing DSSCs or the CuSCN-based BHJ OPVs discussed previously. This motivated experimentation into the use of CuSCN in high-efficiency hybrid photovoltaic devices, such as perovskite-based photovoltaics [149].

PSCs are an emerging third generation photovoltaic technology, where perovskite-based compounds are used as light absorbers. PSCs are now intensely researched due to rapid progress in increasing PCE [150–152]. A common class of perovskites used in photovoltaics are organometal halide perovskites, with ABX_3 perovskite crystal structure. Typically, methylammonium lead halides of the form $CH_3NH_3PbX_3$ are used, where $CH_3NH_3^+$ is the A-site ion and Pb^{2+} is the B-site ion; the halide, X, is typically chlorine (Cl), bromine (Br) or iodine (I). Initially, it was the effective photocurrent generation from $CH_3NH_3PbBr_3$ and $CH_3NH_3PbI_3$ in DSSC-type photovoltaics that demonstrated the light harvesting potential of organometal halide perovskites [153]. Subsequently, high PCE PSCs were developed.

Ordinary DSSCs with dye-sensitized n-ZnO and p-CuSCN HTM show optimized performance when the ZnO-nanorod structure is enhanced with an inorganic perovskite interlayer of p-type bismuth ferrite (BFO) [154]. However, despite the significant increase in device efficiency, the enhanced devices exhibit a very low PCE of 0.217%. Reports of PSCs with CuSCN first emerged in 2014 [71, 80, 126–129], and figure 12 illustrates the typical device structure of a PSC with CuSCN HTM [126]. A glass substrate with a transparent conducting film of FTO functions as the anode; an Au cathode is present at the opposite end of the device. Mesoporous TiO_2 functions as an electron extracting scaffold, and $CH_3NH_3PbI_3$ is the solution-deposited perovskite light absorber. In this case, the solid-state CuSCN HTM is printed by doctor blading. Figure 13(a) shows the J–V characteristics, measured in the dark and under simulated AM1.5G illumination. It was argued that the large hole mobility in CuSCN facilitates significantly higher J_{SC}, and improves charge extraction from $CH_3NH_3PbI_3$ by facilitating rapid hole-transport to the cathode, while small increases were also observed in FF and V_{OC}. Consequently, PCE up to 12.4% was achieved, compared with only 6.7% in the absence of CuSCN [126]. Significant rises in photocurrent in the 450–800 nm spectral region, as observed from IPCE data in figure 13(b), confirms an improvement in the efficiency of charge injection and collection. Several other publications reporting CuSCN-based PSCs with similar efficiencies have also emerged in recent months. For instance, an average PCE of 15.6% was measured in inverted planar structures containing $CH_3NH_3PbI_3$ and electrodeposited CuSCN, with the best-performing devices achieving PCE of 16.6% [155]. The small standard deviation in the measured photovoltaic parameters of 18 solar cells also demonstrates high device reproducibility and hence improved manufacturing yield. Another experiment, which focuses on the benefits of substrate-preheating, succeeds in enhancing the maximum PCE from 5.45 to 10.51% by limiting the diffusion of CuSCN into the

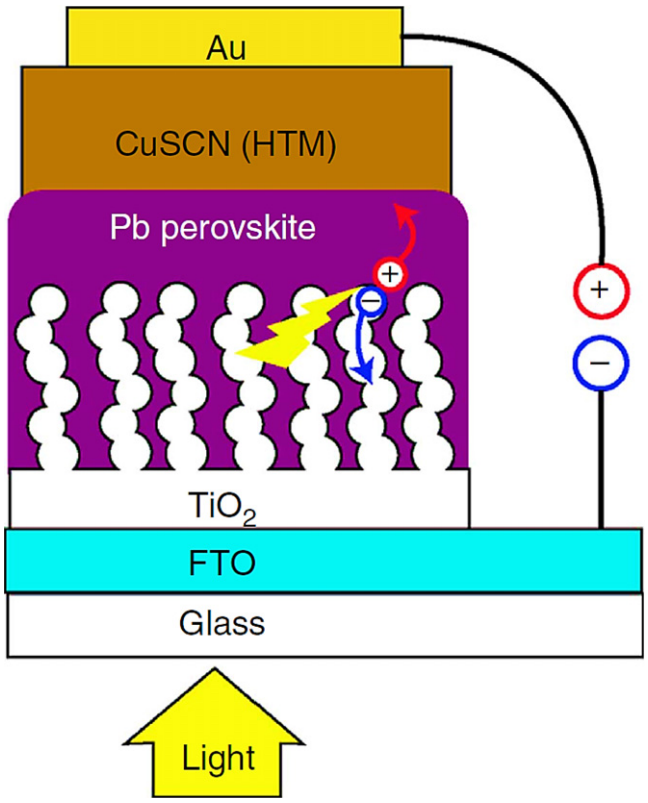

Figure 12. Schematic of a hybrid perovskite solar cell. A TiO_2 electron-extraction scaffold is deposited onto a FTO-coated glass substrate. Holes generated at the $CH_3NH_3PbI_3$ perovskite light absorber are transported to the Au cathode via the CuSCN HTM. Adapted by permission from Macmillan Publishers Ltd: Nature Communications [126], copyright 2014.

$CH_3NH_3PbI_3$ active layer through pinholes that are otherwise present [156]. A second study into reducing interdiffusion between CuSCN and $CH_3NH_3PbI_3$ reported similar results, with PCE measurements reaching 11.96% in the optimized devices [157]. Furthermore, the research on CuSCN appears to be reaching the stage where it is now recongnized as a standard HTM, utilized in experiments on more general scientific problems, such as trap state formation in PSCs [158]

Other studies on PSCs with CuSCN HTM are yet to surpass the 10% PCE margin, but show encouraging results. For instance, printed CuSCN interlayers are also successfully incorporated into $CH_3NH_3PbI_3$-based PSCs, where antimony trisulphide surface blocking layers were found to improve device stability and enhance device lifetime by preventing structural changes to the perovskite material upon exposure to light [128]. Furthermore, there is evidence to suggest that inorganic HTMs, such as printed CuSCN films, limit photovoltaic degradation of moisture-sensitive perovskite materials that can otherwise cause instabilities in high-humidity environments [71]. However, the doctor-blading of CuSCN films as hole conductors for $CH_3NH_3PbI_3$-based PSCs creates a risk of interdiffusion between the absorber and the HTM, which was reported to be the reason for the inferior device performance observed [129]. CuSCN films drop-casted from a DPS solution onto substrates heated to 85 °C, have also

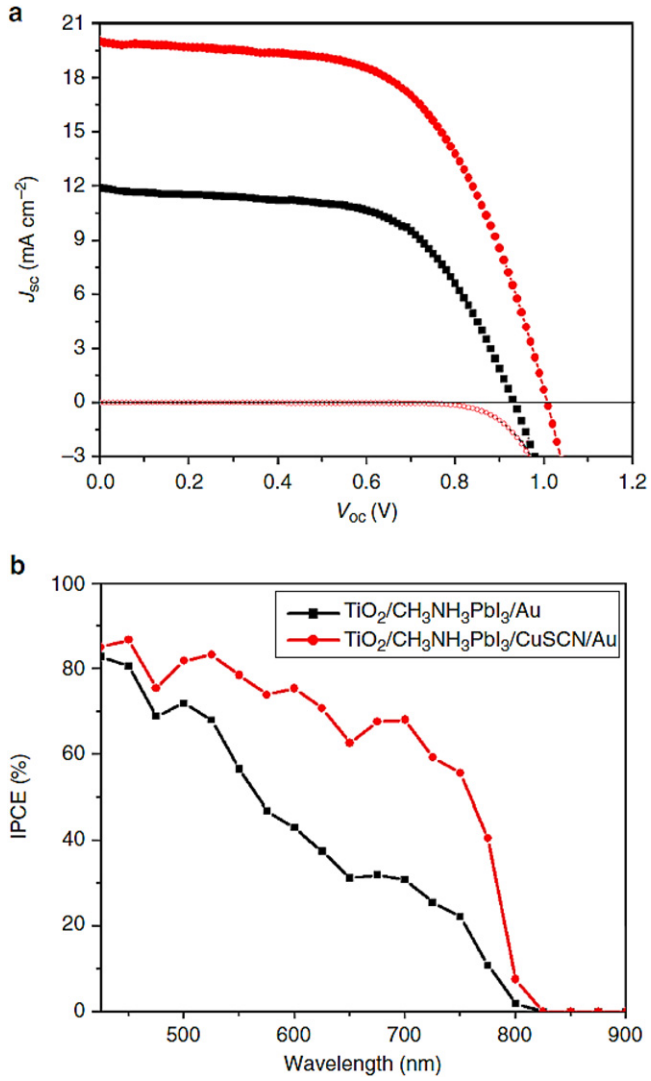

Figure 13. (a) *J–V* characteristics from a $CH_3NH_3PbI_3$ perovskite solar cell, with (circles) and without (squares) CuSCN HTM, measured in the dark and with AM1.5G irradiation. (b) Corresponding IPCE (EQE) spectra of a hybrid perovskite cell shows improved photocurrent with the addition of CuSCN HTM. Reprinted by permission from Macmillan Publishers Ltd: Nature Communications [126], copyright 2014.

been shown to serve as functional HTM interlayers in $CH_3NH_3PbI_{3-x}Cl_x$ based cells with PCE = 6.4% [127]. The extracted FF values of 62% indicate good hole selectivity, but modest V_{OC} values were observed, and explained by recombination losses in both the HTM and perovskite films. In a recent study, however, researchers succeeded in demonstrating electrodeposited CuSCN films as effective HTMs in $CH_3NH_3PbI_{3-x}Cl_x$ based PSCs [80], although PCEs measured with nickel oxide (NiO) interlayers were higher than values achieved with CuSCN.

6. Organic light-emitting diodes (OLEDs)

The digital display market is being revolutionized following breakthroughs in OLED technology, with the emergence of commercialized smartphone, television and tablet products incorporating OLED displays [1, 2, 159, 160]. Reports of lightweight, high-efficiency OLEDs fabricated on flexible, plastic substrates open the door to a wider range of next generation display applications relative to traditional flat panel displays that utilize liquid crystal display (LCD) technology [161]. Moreover, white OLEDs are an environmentally-friendly form of lighting, which shows potential as a major competitor for common incandescent and fluorescence technologies [162], with vacuum processed OLEDs challenging the 100 lm W^{-1} luminous power efficiency of fluorescent lighting [163]. Vacuum processing schemes are certainly not ideal for application in large-area electronics due to their expensive and complicated nature. Consequently, solution-processing techniques for OLED fabrication, such as inkjet printing [164], are gaining interest. Selection of materials for hole injection and transport poses an additional challenge. PEDOT:PSS is the archetypal material, but it suffers from several drawbacks, which include interface instabilities resulting from PEDOT:PSS chemically reacting with organic emissive layers [121] and etching the commonly used ITO anodes [122]. Hence, it is necessary to explore alternative material systems and CuSCN is one such option that appears to satisfy all important requirements including, extremely low cost, processing versatility, extreme optical transparency and excellent hole-transport/electron blocking properties.

6.1. Operating principles of OLEDs

Modern OLEDs employ multilayer device configurations similar to that illustrated in figure 14. Such structures contain distinct ETLs and HTLs, identified as ETL and HTL, respectively, in addition to the all-important emissive layer (EML). The three layers are contained between a high work-function anode, and a low work-function metal cathode that injects holes and electrons into the HTL and ETL, respectively. Light emission originates from an organic EML, while ETL and HTL are often inorganic interlayers with complementary electronic band structures that optimize the device's light-emitting characteristics. The conventional device architecture discussed in this review is the bottom-emitting OLED; top-emitting OLEDs are an alternative architecture and is better suited to some display technologies [165]. Bottom-emitting architectures necessitate the use of transparent substrates, anodes and HTLs. Meanwhile, HTLs must also exhibit good hole-transport and electron blocking characteristics in order to maximize electron-hole recombination and facilitate photon emission. Some HTLs also function as efficient hole-injection layers (HILs), but additional HILs are inserted in some cases. The EML facilitates radiative recombination of electrons and holes, and thus contains highly emissive organic/organo-metallic compounds.

When a voltage is applied to the electrodes, electrons are injected at the cathode and holes are injected at the anode. Pairs of holes and electrons subsequently meet within the EML to form excitons, and it is the decay of excitons within that part of the device that results in optical photon emission. The electroluminescence (EL) can be due to fluorescence or

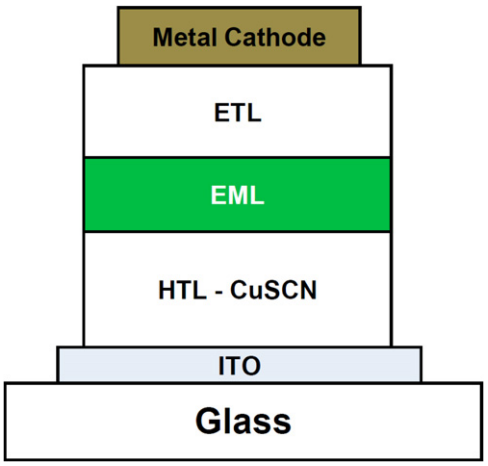

Figure 14. Schematic of a conventional bottom-emitting OLED with a transparent glass substrate, where CuSCN can be used as the HTL. The emissive region is present between the ETL and HTL, with an ITO anode and a metal cathode functioning as top and bottom contacts.

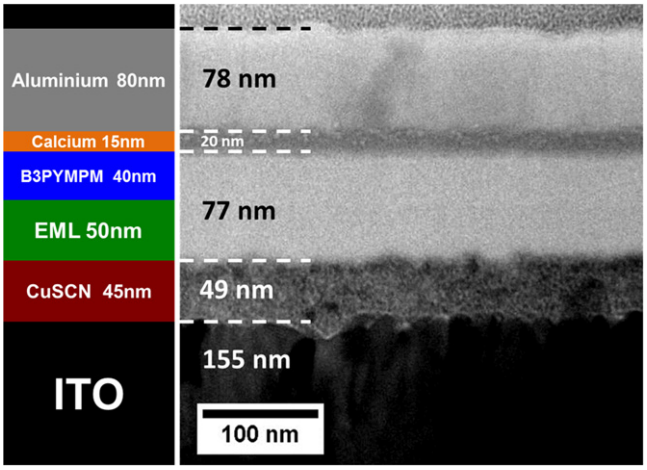

Figure 15. Schematic of an OLED with CuSCN HIL/HTL (left) and corresponding TEM image of a cross-section from the device (right). The OLED contains a small molecule EML, ITO anode, and Ca/Al cathode. The two organic layers, EML and ETL (4,6-bis(3,5-di (pyridin-3-yl)phenyl)-2-methylpyrimidine (B3PYMPM)), are not resolved in the image due to their similar composition limiting scattering contrast. Reprinted with permission from [63], copyright 2014 WILEY-VCH Verlag GmbH & Co. KGaA, Weinheim.

phosphorescence process, where the latter gives greater internal quantum efficiencies (theoretically up to 100%) because electronic transitions that violate spin-related quantum mechanical selection rules also contribute to useful radiative emission [166, 167]. Furthermore, there is often a blend of organic compounds often in the form of guest dopants dispersed within a host system. Peak spectral emission, and thus OLED colour, is mainly tuned by selecting molecules with appropriate HOMO and LUMO levels. OLED display technologies are further categorized according to differences in the driving electronics/schemes employed. Passive-matrix OLEDs employ external circuitry to control rows of pixels. Active-matrix OLEDs (AMOLEDs) are supported by TFT backplanes that control individual pixels; AMOLED displays require, in principle, lower power consumption and are better suited to large-area applications.

OLEDs are characterized using a variety of methods. Measurement of the EL spectrum is of particular importance as it shows a characteristic emission peak that corresponds to the EML composition while the luminance value quantifies the brightness of the device. Reports typically present current density–voltage–luminance (*J–V–L*) characteristics, where current density and luminance are shown as functions of voltage. Important device parameters such as turn-on voltage (V_{ON}) can be extracted directly from the *I–V* characteristics. Next, OLED efficiency parameters are specified. Radiometric efficiency parameters provide an important understanding of device behaviour, but have little relevance for commercial display applications. Consequently, photometric efficiency parameters are often highlighted in the literature, as opposed to variables such as EQE, which defines the number ratio of photon output to charge-carrier input. Luminous efficiency is the ratio between luminance and electrical current (cd A^{-1}); it is a photometric efficiency that accounts for the spectral response of the human eye. Another key parameter is the luminous power efficiency (luminosity), which is the ratio between total luminous flux and electrical power input given in lm W^{-1}.

6.2. OLEDs with CuSCN hole-transporting/electron blocking interlayers

Surprisingly, to date there appears to be only a few reports of OLEDs utilizing CuSCN [63, 168]. The device architecture of solution-processed, multilayer, bottom-emitting, phosphorescent green OLEDs from the earlier study is illustrated in figure 14 [63]. Meanwhile, figure 15 shows a comparison between OLED design and a transmission electron microscope (TEM) image of the focus ion beam-milled cross section of a real OLED. CuSCN HIL/HTLs are spin coated from a DES solution at room temperature resulting in layers with good uniformity. Furthermore, the distinct interface between CuSCN and EML, where the latter is processed from cholorobenzene, demonstrates excellent solvent orthogonality between CuSCN and chlorobenzene. The deep HOMO level of the ETL, combined with the high energy conduction band of CuSCN, confines excitons tightly within the EML while eliminating parasitic charge recombination. Phosphorescent green emission originates from small molecule guest-host blends within the EML. Guest emitter, bis(2-phenylpyridine) (acetylacetonate)iridium(III), commonly known as $(PPy)_2Ir$ (acac), was dispersed within a host that is a blend of two compounds, namely; 2, 6-bis(3-(9H-carbazol-9-yl)phenyl) pyridine and 4, 4′, 4″-tris(N-carbazolyl)triphenylamine (26DCzPPy:TCTA). Energy levels of guests and hosts are aligned such that the combination favours charge-injection and balance.

The photoluminescence (PL) spectrum shown in figure 16(a) reveals a 523 nm emission peak for $(PPy)_2Ir$ (acac) guest emitter [63]. The EL spectra for CuSCN and

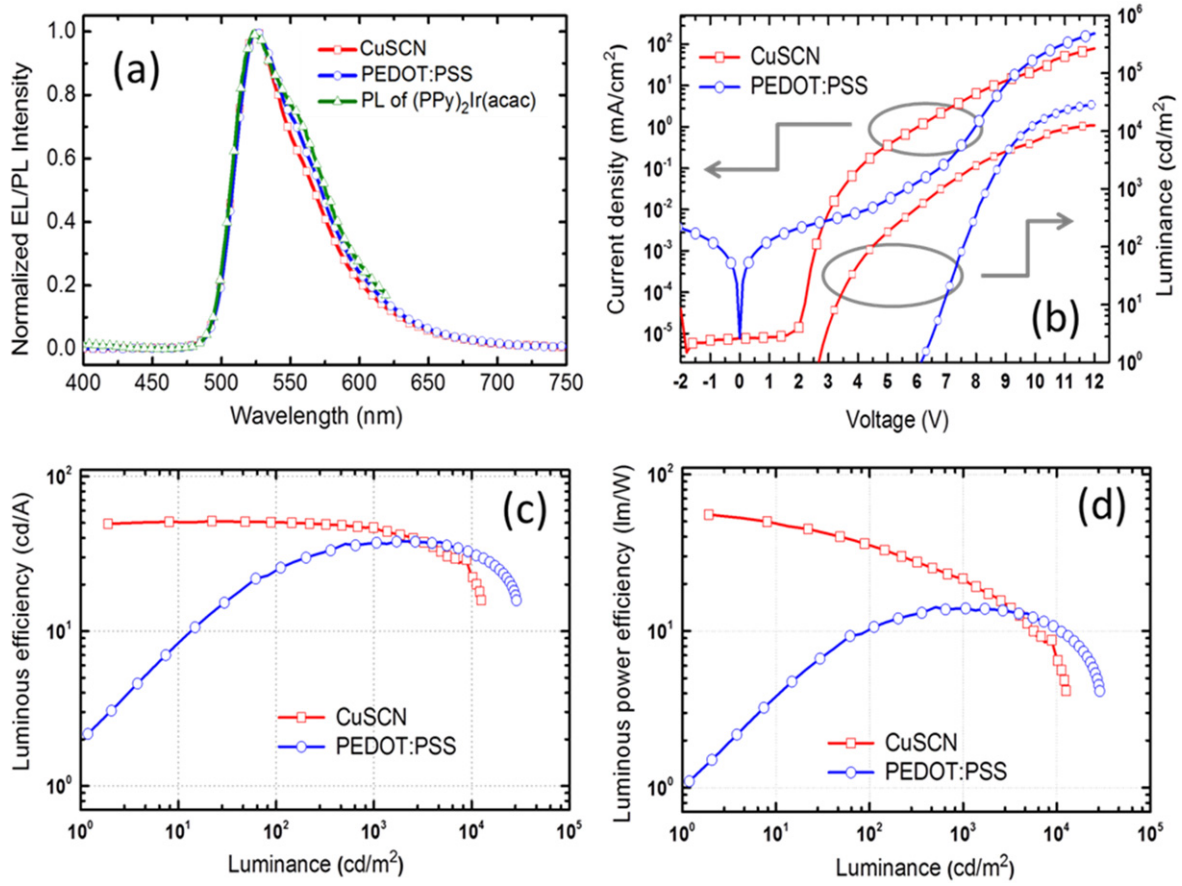

Figure 16. Comparison of results for OLEDs with CuSCN (squares) and PEDOT:PSS (circles) HIL/HTL. (a) EL spectra for $(PPy)_2Ir(acac)$ guest emitter recorded at 0.1 mA, with the PL spectrum of $(PPy)_2Ir(acac)$ shown for reference. (b) *J–V–L* characteristics. (c) Luminous efficiency. (d) Luminous power efficiency. Reprinted with permission from [63], copyright 2014 WILEY-VCH Verlag GmbH & Co. KGaA, Weinheim.

PEDOT:PSS devices closely match the PL spectrum indicating that light emission is primarily determined by the properties of the EML. The *J–V–L* characteristics of the best performing OLEDs are presented in figure 16(b). Interestingly, a higher V_{ON} of ~6 V for PEDOT:PSS devices, determined under forward bias, was observed and attributed to the significant difference between the HOMO of TCTA (5.6 eV) and the work-function of PEDOT:PSS (4.9–5.2 eV). In contrast, the injection barrier for holes is much smaller when CuSCN is used and thus the CuSCN OLEDs show significantly lower V_{ON} of ~2.7 V. Moreover, significantly lower leakage currents are detected in OLEDs with CuSCN due to its excellent electron-blocking properties, a result of its rather high conduction band energy (~2.0 eV). This important characteristic makes inclusion of additional hole-injection or electron-blocking layers completely unnecessary, hence significantly reducing the fabrication cost. Figures 16(c) and (d) display the photometric efficiencies for the two types of cells from which critical performance parameters can be extracted. Luminous efficiency and luminous power efficiency of PEDOT:PSS OLEDs improve with increasing luminance (i.e. higher bias voltages), but CuSCN OLEDs show superior performance in the luminance range relevant to display applications (e.g. $<1000\ cd\ m^{-2}$). Not surprisingly, the luminous and luminous power efficiencies of CuSCN-based OLEDs were found to exceed those of PEDOT:PSS devices at both $100\ cd\ m^{-2}$ and $1000\ cd\ m^{-2}$ luminance levels. Maximum luminance values in CuSCN-based OLEDs exceed $10\,000\ cd\ m^{-2}$ with the highest luminous and luminous power efficiencies on the order of $\sim 51\ cd\ A^{-1}$ and $\sim 55\ lm\ W^{-1}$, respectively. Most importantly, the latter two values are significantly greater than efficiencies achieved in PEDOT:PSS-based OLEDs.

A more recent publication on solution-processed, phosphorescent OLEDs reports on the use of CuSCN as the HTL and PEDOT:PSS as the HIL in devices based on metal cluster complexes [168]. The ETL utilizes a mixed host with hole-transporting 1,3-di(9H-carbazol-9-yl) benzene) [mCP] and electron-transporting 1,3-bis(5-(4-(tert-butyl)phenyl)-1,3,4-oxadiazol-2-yl)-benzene) [OXD-7], doped with an Au_4Ag_2 cluster complex as the phosphorescent emitter. Five different Au_4Ag_2 cluster complexes were studied and used to fabricate OLEDs with emission peaks in the 482–550 nm wavelength range. The addition of the solution-processed CuSCN HTL was found to significantly reduce the turn-on voltage of the OLEDs and increase their electroluminescent efficiency. High-performance CuSCN-based OLEDs were thus produced with the following maximum efficiency parameters: luminous

efficiency of 24.1 cd A^{-1}, luminous power efficiency of 11.6 lm W^{-1}, and EQE of 7.0%.

Despite the much promising achievements, however, solution-processed OLEDs incorporating CuSCN as the HIL/HTL are yet unable to compete with state-of-the-art vacuum-processed OLEDs [160, 169]. It is certain however that further optimization of solution-processable interlayer technologies based on CuSCN, as well as other materials systems, is expected to improve the efficiency of solution-processed OLEDs, and potentially enable use of the technology in a range of inexpensive lighting applications.

7. Conclusions

A review of the literature on the wide bandgap semiconductor CuSCN reveals that it is a highly versatile p-type electronic material with significant potential for a host of relevant applications. Its excellent hole-transport characteristics, combined with its low-temperature solution-processability, make CuSCN a strong contender as hole-injecting/hole-transport interlayer material in next-generation plastic optoelectronics. Thus far, the wide bandgap and the relatively high hole mobility of CuSCN has been explored in high-efficiency organic and hybrid photovoltaic cells, and OLEDs. Furthermore, the first CuSCN transistors and integrated circuits with promising performance characteristics close to those required for use in driving backplanes for various optical display technologies and future transparent microelectronics, have also been developed. Most importantly, a range of scalable, low-cost techniques suitable for large-area deposition of CuSCN have been demonstrated, including, printing (e.g. inkjet printing and doctor blading), spin-coating, spray-coating, and low-temperature electrochemical deposition. By exploring this unique combination of highly desirable physical characteristics, numerous studies have demonstrated high performance CuSCN-based opto/electronic devices even on inexpensive flexible substrates.

Results reported in the literature to date are most definitely very promising. For instance, organic solar cells and OLEDs incorporating CuSCN as hole-transporting layers, typically exhibit efficiencies that are often far superior to those measured for devices based on conventional hole-transporting materials such as the conductive polymer PEDOT:PSS. Hole-transporting interlayers based on CuSCN have also shown excellent hole-injecting/extracting and electron blocking properties. In the case of OLEDs, this important characteristic results in devices with significantly lower turn-on voltages, while in the case of organic solar cells, it leads to significantly reduced reverse currents and higher device performance.

However, some challenges still lie ahead. In many cases, research on CuSCN HTLs is at an early stage. Therefore, the origins of certain intrinsic properties, such as the nature of its bandgap and hole-mobility limitations, are yet to be fully understood. While significant efforts are being made to improve the efficiency of CuSCN-based organic and hybrid systems, further optimization of fabrication parameters is required to compete with existing products. For instance, inorganic photovoltaic cells and vacuum-processed OLEDs are commercially available products, but all CuSCN-based device applications reported to date are still far from being used in a commercial product. Recent advances, however, have provided greater insights into factors that affect the performance of CuSCN interlayers, and as such significant progress is being made, with the number of articles published annually on high performance CuSCN-based devices steadily on the rise. This is particularly true in the case of emerging technologies, such as PSCs, as well as more established technologies such as OLEDs. Meanwhile, researchers should continue to focus on gaining a deeper understanding of the underlying physical mechanisms that govern the semiconducting behaviour of CuSCN in order to realize the full capabilities of this rather interesting and much promising material system. If such efforts are successful, CuSCN and possibly other related compounds, have the potential to serve as universal transparent hole-transporting/electron-blocking semiconductors and potentially dominate numerous existing, as well as rapidly emerging, opto/electronic applications.

References

[1] Thejo Kalyani N and Dhoble S J 2012 Organic light emitting diodes: energy saving lighting technology—a review *Renew. Sustain. Energy Rev.* **16** 2696–723
[2] Geffroy B, le Roy P and Prat C 2006 Organic light-emitting diode (OLED) technology: materials, devices and display technologies *Polym. Int.* **55** 572–82
[3] Hoppe H and Sariciftci N S 2004 Organic solar cells : an overview *J. Mater. Res.* **19** 1924–45
[4] Günes S and Sariciftci N S 2008 Hybrid solar cells *Inorg. Chim. Acta* **361** 581–8
[5] Fortunato E, Barquinha P and Martins R 2012 Oxide semiconductor thin-film transistors: a review of recent advances *Adv. Mater.* **24** 2945–86
[6] Kwon J-Y, Lee D-J and Kim K-B 2011 Review paper: transparent amorphous oxide semiconductor thin film transistor *Electron. Mater. Lett.* **7** 1–11
[7] Nomura K, Ohta H, Takagi A, Kamiya T, Hirano M and Hosono H 2004 Room-temperature fabrication of transparent flexible thin-film transistors using amorphous oxide semiconductors *Nature* **432** 488–92
[8] Tate J and Keszler D A 2010 p-Type wide-band-gap semiconductors for transparent electronics *Transparent Electronics: From Synthesis to Applications* ed A Facchetti and T Marks (Chichester, UK: Wiley) pp 61–82
[9] Mahan G D 1965 Van der waals forces in solids *J. Chem. Phys.* **43** 1569
[10] Darling S B and You F 2013 The case for organic photovoltaics *RSC Adv.* **3** 17633
[11] Yeh N and Yeh P 2013 Organic solar cells: their developments and potentials *Renew. Sustain. Energy Rev.* **21** 421–31
[12] Caraveo-Frescas J, Nayak P, Al-Jawhari H, Granato D, Schwingenschloegl U and Alshareef H 2013 Record mobility in transparent p-type tin monoxide films and devices by phase engineering *ACS Nano* **7** 5160–7
[13] Nomura K, Ohta H, Ueda K, Kamiya T, Hirano M and Hosono H 2003 Thin-film transistor fabricated in single-crystalline transparent oxide semiconductor *Science* **300** 1269–72

[14] Nandy S, Banerjee A, Fortunato E and Martins R 2013 A review on Cu_2O and CuI-based p-type semiconducting transparent oxide materials: promising candidates for new generation oxide based electronics *Rev. Adv. Sci. Eng.* **2** 273–304
[15] Fortunato E, Figueiredo V, Barquinha P, Elamurugu E, Barros R, Gonçalves G, Park S-H K, Hwang C-S and Martins R 2010 Thin-film transistors based on p-type Cu_2O thin films produced at room temperature *Appl. Phys. Lett.* **96** 192102
[16] Muñoz-Rojas D, Jordan M, Yeoh C, Marin A T, Kursumovic A, Dunlop L A, Iza D C, Chen A, Wang H and MacManus Driscoll J L 2012 Growth of 5 cm^2 V^{-1} s^{-1} mobility, p-type copper(I) oxide (Cu_2O) films by fast atmospheric atomic layer deposition (AALD) at 225 °C and below *AIP Adv.* **2** 042179
[17] Zou X, Fang G, Yuan L and Li M 2010 Top-gate low-threshold voltage thin-film transistor grown on substrate using a high-k HfON gate dielectric *IEEE Electron Device Lett.* **31** 827–9
[18] Blue R and Mathers F 1933 Electrodeposition of metals and alloys from formamide solutions *J. Electrochem. Soc.* **63** 231–8
[19] Tanaka N and Takamura T 1959 Spectrophotometric studies on thiocyanatocuprate (II) complexes in aqueous solution *J. Inorg. Nucl. Chem.* **9** 15–23
[20] Hunter J, Massie W, Meiklejohn J and Reid J 1969 Thermal rearrangement in copper(II) thiocyanate *Inorg. Nucl. Chem. Lett.* **5** 1–4
[21] Hollebone B and Nyholm R 1971 Pseudo-halide complexes of transition metals: I. Synthesis and properties of cobalt (II), nickel (II), copper (II), and zinc (II) derivatives *J. Chem. Soc.* A 332–6
[22] Hollebone B 1971 Pseudo-halide complexes of transition metals: II. Spectra, structure, and nature of bonding *J. Chem. Soc.* A 461–86
[23] Kabešová M, Dunaj-Jurčo M and Serator M 1976 The crystal structure of copper (I) thiocyanate and its relation to the crystal structure of copper (II) diammine dithiocyanate complex *Inorg. Chim. Acta* **17** 161–5
[24] Jaffe J E, Kaspar T C, Droubay T C, Varga T, Bowden M E and Exarhos G J 2010 Electronic and defect structures of CuSCN *J. Phys. Chem.* C **114** 9111–7
[25] Pattanasattayavong P, Ndjawa G O N, Zhao K, Chou K W, Yaacobi-Gross N, O'Regan B C, Amassian A and Anthopoulos T D 2013 Electric field-induced hole transport in copper(I) thiocyanate (CuSCN) thin-films processed from solution at room temperature *Chem. Commun.* **49** 4154–6
[26] Tennakone K, Jayatissa A H, Fernando C A N, Wickramanayake S, Punchihewa S, Weerasena L K and Premasiri W D R 1987 Semiconducting and photoelectrochemical properties of n-and p-type β-CuCNS *Phys. Status Solidi* a **103** 491–7
[27] Ji W, Yue G-Q, Ke F-S, Wu S, Zhao H-B, Chen L-Y, Wang S-Y and Jia Y 2012 Electronic structures and optical properties of CuSCN with Cu vacancies *J. Korean Phys. Soc.* **60** 1253–7
[28] Ptaszynski B, Skiba E and Krystek J 1998 Thermal decomposition of alkali metal, copper(I) and silve(I) thiocyanates *Thermochim. Acta* **319** 75–85
[29] Rietman E 1985 Conduction properties of silver and copper pseudohalides *J. Mater. Sci. Lett.* **4** 5–7
[30] Pattanasattayavong P, Yaacobi-Gross N, Zhao K, Ndjawa G O N, Li J, Yan F, O'Regan B C, Amassian A and Anthopoulos T D 2013 Hole-transporting transistors and circuits based on the transparent inorganic semiconductor copper(I) thiocyanate (CuSCN) processed from solution at room temperature *Adv. Mater.* **25** 1504–9
[31] Wu W, Jin Z, Hua Z, Fu Y and Qiu J 2005 Growth mechanisms of CuSCN films electrodeposited on ITO in EDTA-chelated copper(II) and KSCN aqueous solution *Electrochim. Acta* **50** 2343–9
[32] Ni Y, Jin Z and Fu Y 2007 Electrodeposition of p-type CuSCN thin films by a new aqueous electrolyte with triethanolamine chelation *J. Am. Ceram. Soc.* **90** 2966–73
[33] Gao X-D, Li X-M, Yu W-D, Qiu J-J and Gan X-Y 2008 Room-temperature deposition of nanocrystalline CuSCN film by the modified successive ionic layer adsorption and reaction method *Thin Solid Films* **517** 554–9
[34] Yaacobi-Gross N, Treat N D, Pattanasattayavong P, Faber H, Perumal A K, Stingelin N, Bradley D D C, Stavrinou P N, Heeney M and Anthopoulos T D 2015 High-efficiency organic photovoltaic cells based on the solution-processable hole transporting interlayer copper thiocyanate (CuSCN) as a replacement for PEDOT:PSS *Adv. Energy Mater.* **5**
[35] Pattanasattayavong P, Thomas S, Adamopoulos G, McLachlan M A and Anthopoulos T D 2013 p-channel thin-film transistors based on spray-coated Cu_2O films *Appl. Phys. Lett.* **102** 163505
[36] Jayaweera P V V, Perera A G U, Senevirathna M K I, Pitigala P K D D P and Tennakone K 2004 Dye-sensitized near-infrared room-temperature photovoltaic photon detectors *Appl. Phys. Lett.* **85** 5754
[37] Tennakone K, Wickramanayaka S and Basu S 1985 Cuprous thiocyanate: a superior photocatalyst for oxidation of water *Chem. Phys. Lett.* **121** 551–3
[38] Tennakone K and Kahanda M 1984 Dye sensitization of cuprous thiocyanate photocathode in aqueous KCNS *J. Electrochem. Soc.* **131** 1574–7
[39] Wu W B, Jin Z G, Hu G D and Bu S J 2007 Electrochemical deposition of p-type CuSCN in porous n-type TiO_2 films *Electrochim. Acta* **52** 4804–8
[40] Hatch S M, Briscoe J and Dunn S 2013 A self-powered ZnO-nanorod/CuSCN UV photodetector exhibiting rapid response *Adv. Mater.* **25** 867–71
[41] Li S, Xu J, Shi S, Shi X, Wang X, Wang C, Zhang X, Liu Z and Li L 2015 UV photoresponse properties of ZnO nanorods arrays deposited with CuSCN by SILAR method *Chem. Phys. Lett.* **620** 50–5
[42] Garnier J, Parize R, Appert E, Chaix-Pluchery O, Kaminski-Cachopo A and Consonni V 2015 Physical properties of annealed ZnO nanowire/CuSCN heterojunctions for self-powered UV photodetectors *ACS Appl. Mater. Interfaces* **7** 5820–9
[43] Fernando C A N, Priyankara W T C and Dharmadasa I M 2002 Photocurrent enhancement of interlocked LB film dye layers in a p-CuSCN sensitised photoelectrochemical cell *Renew Energy* **25** 69–79
[44] Fernando C and Kitagawa A 1994 Photoelectrochemical properties of rhodamine-C 18 sensitized p-CuSCN photoelectrochemical cell (PEC) *Sol. Energy Mater. Sol. Cells* **33** 301–15
[45] Fernando C A N, Takahashi K, Kitagawa A, Suzuki M, Wethasinghe S K and Kumarawadu I 2001 Remarkable stability of the enhanced sharp photocurrent in methylviolet–C18 and rhodamine–C18 dye-sensitized photoelectrochemical cell with p-CuSCN *Sol. Energy Mater. Sol. Cells* **69** 345–52
[46] Tennakone K, Kumarasinghe A R, Sirimanne P M and Kumara G R R A 1995 Deposition of thin polycrystalline films of cuprous thiocyanate on conducting glass and photoelectrochemical dye-sensitization *Thin Solid Films* **261** 307–10
[47] Grätzel M 2001 Photoelectrochemical cells *Nature* **414** 338–44

[48] O'Regan B and Schwartz D 1998 Large enhancement in photocurrent efficiency caused by UV illumination of the dye-sensitized heterojunction TiO_2/RuLL'NCS/CuSCN: Initiation and potential *Chem. Mater.* **10** 1501–9
[49] O'Regan B and Schwartz D 1995 Efficient photo-hole injection from adsorbed cyanine dyes into electrodeposited copper (I) thiocyanate thin films *Chem. Mater.* **7** 1349–54
[50] O'Regan B and Schwartz D T 1996 Efficient dye-sensitized charge separation in a wide-band-gap p–n heterojunction *J. Appl. Phys.* **80** 4749
[51] Sun L, Huang Y, Anower Hossain M, Li K, Adams S and Wang Q 2012 Fabrication of TiO_2/CuSCN bulk heterojunctions by profile-controlled electrodeposition *J. Electrochem. Soc.* **159** D323
[52] Marí B, Singh K C, Ortiz L and Mollar M 2012 Electrochemical fabrication and characterization of p-CuSCN/n-ZnO heterojunction devices *J. Solid State Electrochem.* **17** 667–73
[53] Xiong C, Yao R H, Wan W J and Xu J X 2014 Fabrication and electrical characterization of ZnO rod arrays/CuSCN heterojunctions *Optik* **125** 785–8
[54] Bacaksiz E, Aksu S, Çankaya G, Yılmaz S, Polat İ, Küçükömeroğlu T and Varilci A 2011 Fabrication of p-type CuSCN/n-type micro-structured ZnO heterojunction structures *Thin Solid Films* **519** 3679–85
[55] Gertman R, Berger Y and Visoly-Fisher I 2014 Pulsed electrodeposition of CuSCN for superfilling of ZnO nanowire array electrodes *Electrochim. Acta* **125** 65–70
[56] Wu W, Cui S, Yang C, Hu G and Wu H 2009 Electrochemically superfilling of n-type ZnO nanorod arrays with p-type CuSCN semiconductor *Electrochem. commun.* **11** 1736–9
[57] Ni Y, Jin Z, Yu K, Fu Y, Liu T and Wang T 2008 Electrochemical deposition characteristics of p-CuSCN on n-ZnO rod arrays films *Electrochim. Acta* **53** 6048–54
[58] Hatch S M, Briscoe J and Dunn S 2013 Improved CuSCN–ZnO diode performance with spray deposited CuSCN *Thin Solid Films* **531** 404–7
[59] Aé L, Chen J and Lux-Steiner M C 2008 Hybrid flexible vertical nanoscale diodes prepared at low temperature in large area *Nanotechnology* **19** 475201
[60] Lévy-Clément C, Tena-Zaera R, Ryan M A, Katty A and Hodes G 2005 CdSe-sensitized p-CuSCN/nanowire n-ZnO heterojunctions *Adv. Mater.* **17** 1512–5
[61] Zhang Q, Guo H, Feng Z, Lin L, Zhou J and Lin Z 2010 n-ZnO nanorods/p-CuSCN heterojunction light-emitting diodes fabricated by electrochemical method *Electrochim. Acta* **55** 4889–94
[62] Ogawa Y, White M S, Sun L, Scharber M C, Sariciftci N S and Yoshida T 2014 Substrate-oriented nanorod scaffolds in polymer-fullerene bulk heterojunction solar cells *Chem. Phys. Chem.* **15** 1070–5
[63] Perumal A, Faber H, Yaacobi-Gross N, Pattanasattayavong P, Burgess C, Jha S, McLachlan M A, Stavrinou P N, Anthopoulos T D and Bradley D D C 2014 High-efficiency, solution-processed, multilayer phosphorescent organic light-emitting diodes with a copper thiocyanate hole-injection/hole-transport layer *Adv. Mater.* **27** 93–100
[64] Kumara G R R A, Konno A, Senadeera G K R, Jayaweera P V V, De Silva D B R A and Tennakone K 2001 Dye-sensitized solar cell with the hole collector p-CuSCN deposited from a solution in n-propyl sulphide *Sol. Energy Mater. Sol. Cells* **69** 195–9
[65] Tsujimoto K, Nguyen D-C, Ito S, Nishino H, Matsuyoshi H, Konno A, Kumara G R A and Tennakone K 2012 TiO_2 surface treatment effects by Mg^{2+}, Ba^{2+}, and Al^{3+} on Sb_2S_3 extremely thin absorber solar cells *J. Phys. Chem.* C **116** 13465–71
[66] O'Regan B, Lenzmann F, Muis R and Wienke J 2002 A solid-state dye-sensitized solar cell fabricated with pressure-treated P25-TiO_2 and CuSCN: analysis of pore filling and IV characteristics *Chem. Mater.* **14** 5023–9
[67] Carryon G, Le T, Madjidi H, Baxter J and Sun Y 2010 Inkjet printing of inorganic solar cells, *MRS Proc. 1288E*
[68] Zhang X, Yoshioka S, Loew N and Ihara M 2014 Microstructure control of absorber Sb2S3 and p-type semiconductor CuSCN for semiconductor-sensitized solar cells (TiO_2/Sb_2S_3/CuSCN) *ECS Trans. 64* **64** 1–13
[69] Yoshioka S, Mishima T and Ihara M 2013 The effect of TiO_2 microstructure and introduction of silver nanoparticles on conversion efficiency of Sb_2S_3 sensitized semiconductor solar cells *ECS Trans. 50* **50** 33–44
[70] Ito S, Tsujimoto K, Nguyen D-C, Manabe K and Nishino H 2013 Doping effects in Sb_2S_3 absorber for full-inorganic printed solar cells with 5.7% conversion efficiency *Int. J. Hydrogen Energy* **38** 16749–54
[71] Ito S, Tanaka S, Vahlman H, Nishino H, Manabe K and Lund P 2014 Carbon-double-bond-free printed solar cells from TiO_2/$CH_3NH_3PbI_3$/CuSCN/Au: structural control and photoaging effects *Chem. Phys. Chem.* **15** 1194–200
[72] Thomas S R, Pattanasattayavong P and Anthopoulos T D 2013 Solution-processable metal oxide semiconductors for thin-film transistor applications *Chem. Soc. Rev.* **42** 6910–23
[73] Ghosh S and Sarkar S K 2014 Controlled morphology of electrochemically deposited CuSCN by variation of applied bias voltage *Energy Proc.* **54** 777–81
[74] Sirimanne P M and Zhang J B 2008 Characterization of electrochemically prepared CuSCN films and their capabilities of application in dye sensitized photovoltaic cells *Sri Lankan J. Phys.* **9** 19–26
[75] Iwamoto T, Ogawa Y, Sun L, White M S, Glowacki E D, Scharber M C, Sariciftci N S, Manseki K, Sugiura T and Yoshida T 2014 Electrochemical self-assembly of nanostructured CuSCN/rhodamine B hybrid thin film and its dye-sensitized photocathodic properties *J. Phys. Chem.* C **118** 16581–90
[76] Sanchez S, Chappaz-Gillot C, Salazar R, Muguerra H, Arbaoui E, Berson S, Lévy-Clément C and Ivanova V 2012 Comparative study of ZnO and CuSCN semiconducting nanowire electrodeposition on different substrates *J. Solid State Electrochem.* **17** 391–8
[77] Selk Y, Yoshida T and Oekermann T 2008 Variation of the morphology of electrodeposited copper thiocyanate films *Thin Solid Films* **516** 7120–4
[78] Paunovic M and Schlesinger M 2006 *Fundamentals of Electrochemical Deposition* (Hoboken, NJ: Wiley)
[79] Huang M-C, Wang T, Tseng Y-T, Wu C-C, Lin J-C, Hsu W-Y, Chang W-S, Chen I-C and Peng K-C 2015 Influence of annealing on microstructural and photoelectrochemical characteristics of CuSCN thin films via electrochemical process *J. Alloys Compd.* **622** 669–75
[80] Subbiah A S, Halder A, Ghosh S, Mahuli N, Hodes G and Sarkar S K 2014 Inorganic hole conducting layers for perovskite-based solar cells *J. Phys. Chem. Lett.* **5** 1748–53
[81] Chappaz-Gillot C, Berson S, Salazar R, Lechêne B, Aldakov D, Delaye V, Guillerez S and Ivanova V 2014 Polymer solar cells with electrodeposited CuSCN nanowires as new efficient hole transporting layer *Sol. Energy Mater. Sol. Cells* **120** 163–7
[82] Chappaz-Gillot C, Salazar R, Berson S and Ivanova V 2012 Room temperature template-free electrodeposition of CuSCN nanowires *Electrochem. Commun.* **24** 1–4
[83] Chappaz-Gillot C, Salazar R, Berson S and Ivanova V 2013 Insights into CuSCN nanowire electrodeposition on flexible substrates *Electrochim. Acta* **110** 375–81
[84] Street R A 2009 Thin-film transistors *Adv. Mater.* **21** 2007–22

[85] Nayak P K, Caraveo-Frescas J A, Wang Z, Hedhili M N, Wang Q X and Alshareef H N 2014 Thin film complementary metal oxide semiconductor (CMOS) device using a single-step deposition of the channel layer *Sci. Rep.* **4** 4672
[86] Gelinck G, Heremans P, Nomoto K and Anthopoulos T D 2010 Organic transistors in optical displays and microelectronic applications *Adv. Mater.* **22** 3778–98
[87] Shockley W 1950 *Electrons and Holes in Semiconductors* (Princeton, New York: D Van Nostrad Company, Inc.)
[88] Tsuji H, Kamakura Y and Taniguchi K 2010 Drain current model for thin-film transistors with interface trap states *J. Appl. Phys.* **107** 034502
[89] Kim C, Bonnassieux Y and Horowitz G 2011 Fundamental benefits of the staggered geometry for organic field-effect transistors *IEEE Electron Device Lett.* **32** 1302–4
[90] Street R and Salleo A 2002 Contact effects in polymer transistors *Appl. Phys. Lett.* **81** 2887–9
[91] Ishii H and Yamada K 1967 Effects of traps on thin film transistors *Solid State Electron.* **10** 1201–12
[92] Ameri T, Khoram P, Min J and Brabec C J 2013 Organic ternary solar cells: a review *Adv. Mater.* **25** 4245–66
[93] Carlé J E and Krebs F C 2013 Technological status of organic photovoltaics (OPV) *Sol. Energy Mater. Sol. Cells* **119** 309–10
[94] Kumar P and Chand S 2012 Recent progress and future aspects of organic solar cells *Prog. Photovolt., Res. Appl.* **20** 377–415
[95] Xue J 2010 Perspectives on organic photovoltaics *Polym. Rev.* **50** 411–9
[96] Delgado J L, Bouit P-A, Filippone S, Herranz M A and Martín N 2010 Organic photovoltaics: a chemical approach *Chem. Commun.* **46** 4853–65
[97] Ameri T, Li N and Brabec C J 2013 Highly efficient organic tandem solar cells: a follow up review *Energy Environ. Sci.* **6** 2390
[98] Chandrasekaran J, Nithyaprakash D, Ajjan K B, Maruthamuthu S, Manoharan D and Kumar S 2011 Hybrid solar cell based on blending of organic and inorganic materials—an overview *Renew. Sustain. Energy Rev.* **15** 1228–38
[99] Moulé A J, Chang L, Thambidurai C, Vidu R and Stroeve P 2012 Hybrid solar cells: basic principles and the role of ligands *J. Mater. Chem.* **22** 2351
[100] Wright M and Uddin A 2012 Organic–inorganic hybrid solar cells: a comparative review *Sol. Energy Mater. Sol. Cells* **107** 87–111
[101] Weickert J, Dunbar R B, Hesse H C, Wiedemann W and Schmidt-Mende L 2011 Nanostructured organic and hybrid solar cells *Adv. Mater.* **23** 1810–28
[102] Lattante S 2014 Electron and hole transport layers: their use in inverted bulk heterojunction polymer solar cells *Electronics* **3** 132–64
[103] Janssen R A J and Nelson J 2013 Factors limiting device efficiency in organic photovoltaics *Adv. Mater.* **25** 1847–58
[104] Schlenker C W and Thompson M E 2011 The molecular nature of photovoltage losses in organic solar cells *Chem. Commun.* **47** 3702–16
[105] Service R 2011 Outlook brightens for plastic solar cells *Science* **332** 293
[106] Cnops K, Rand B P, Cheyns D, Verreet B, Empl M A and Heremans P 2014 8.4% efficient fullerene-free organic solar cells exploiting long-range exciton energy transfer *Nat. Commun.* **5** 3406
[107] Tennakone K and Kumara G 1998 Nanoporous n-TiO_2/selenium/p-CuCNS photovoltaic cell *J. Phys. D: Appl. Phys.* **31** 2326–30
[108] Nezu S, Larramona G, Choné C, Jacob A, Delatouche B, Péré D and Moisan C 2010 Light soaking and gas effect on nanocrystalline TiO_2/Sb_2S_3/CuSCN photovoltaic cells following extremely thin absorber concept *J. Phys. Chem.* C **114** 6854–9
[109] Boix P and Larramona G 2011 Hole transport and recombination in all-solid Sb_2S_3-sensitized TiO_2 solar cells using CuSCN as hole transporter *J. Phys. Chem.* C **116** 1579–87
[110] Tena-Zaera R, Katty A, Bastide S, Lévy-Clément C, O'Regan B and Muñoz-Sanjosé V 2005 ZnO/CdTe/CuSCN, a promising heterostructure to act as inorganic ETA-solar cell *Thin Solid Films* **483** 372–7
[111] Tena-Zaera R, Ryan M A, Katty A, Hodes G, Bastide S and Lévy-Clément C 2006 Fabrication and characterization of ZnO nanowires/CdSe/CuSCN ETA-solar cell *C. R. Chim.* **9** 717–29
[112] Edri E, Cohen H and Hodes G 2013 Band alignment in partial and complete ZnO/ZnS/CdS/CuSCN extremely thin absorber cells: an x-ray photoelectron spectroscopy study *Appl. Mater. Interfaces* **5** 5156–64
[113] Dittrich T, Kieven D, Belaidi A, Rusu M, Tornow J, Schwarzburg K and Lux-Steiner M C 2009 Formation of the charge selective contact in solar cells with extremely thin absorber based on ZnO-nanorod/In 2S3/CuSCN *J. Appl. Phys.* **105** 034509
[114] Dittrich T, Kieven D, Rusu M, Belaidi A, Tornow J, Schwarzburg K and Lux-Steiner M 2008 Current–voltage characteristics and transport mechanism of solar cells based on ZnO nanorods/In2S3/CuSCN *Appl. Phys. Lett.* **93** 053113
[115] Kieven D, Dittrich T, Belaidi A, Tornow J, Schwarzburg K, Allsop N and Lux-Steiner M 2008 Effect of internal surface area on the performance of ZnO/In2S3/CuSCN solar cells with extremely thin absorber *Appl. Phys. Lett.* **92** 153107
[116] Chen G, Wang L, Zou Y, Sheng X, Liu H, Pi X and Yang D 2011 CdSe quantum dots sensitized mesoporous TiO_2 solar cells with CuSCN as solid-state electrolyte *J. Nanomater* **2011** 269591
[117] Briscoe J, Gallardo D E, Hatch S, Lesnyak V, Gaponik N and Dunn S 2011 Enhanced quantum dot deposition on ZnO nanorods for photovoltaics through layer-by-layer processing *J. Mater. Chem.* **21** 2517
[118] Pivrikas A, Sariciftci N, Juska G and Osterbacka R 2007 A review of charge transport and recombination in polymer/fullerene organic solar cells *Prog. Photovolt., Res. Appl.* **15** 677–96
[119] Brabec C J, Gowrisanker S, Halls J J M, Laird D, Jia S and Williams S P 2010 Polymer-fullerene bulk-heterojunction solar cells *Adv. Mater.* **22** 3839–56
[120] Deibel C, Dyakonov V and Brabec C J 2010 Organic bulk-heterojunction solar cells *IEEE J. Sel. Top. Quantum Electron.* **16** 1517–27
[121] Garcia A, Welch G C, Ratcliff E L, Ginley D S, Bazan G C and Olson dc 2012 Improvement of interfacial contacts for new small-molecule bulk-heterojunction organic photovoltaics *Adv. Mater.* **24** 5368–73
[122] De Jong M P, van IJzendoorn L J and de Voigt M J A 2000 Stability of the interface between indium-tin-oxide and poly (3, 4-ethylenedioxythiophene)/poly(styrenesulfonate) in polymer light-emitting diodes *Appl. Phys. Lett.* **77** 2255
[123] Takahashi K, Suzaka S, Sigeyama Y, Yamaguchi T, Nakamura J and Murata K 2007 Efficiency increase by insertion of electrodeposited CuSCN layer into ITO/organic solid interface in bulk hetero-junction solar cells consisting of polythiophene and fullerene *Chem. Lett.* **36** 762–3
[124] Eerenstein W, Slooff L H, Veenstra S C and Kroon J M 2008 Optical modeling as optimization tool for single and double junction polymer solar cells *Thin Solid Films* **516** 7188–92

[125] Hardin B E, Snaith H J and McGehee M D 2012 The renaissance of dye-sensitized solar cells *Nat. Photonics* **6** 162–9
[126] Qin P, Tanaka S, Ito S, Tetreault N, Manabe K, Nishino H, Nazeeruddin M K and Grätzel M 2014 Inorganic hole conductor-based lead halide perovskite solar cells with 12.4% conversion efficiency *Nat. Commun.* **5** 3834
[127] Chavhan S, Miguel O, Grande H-J, Gonzalez-Pedro V, Sánchez R S, Barea E M, Mora-Seró I and Tena-Zaera R 2014 Organo-metal halide perovskite-based solar cells with CuSCN as the inorganic hole selective contact *J. Mater. Chem.* A **2** 12754
[128] Ito S and Tanaka S 2014 Effects of surface blocking layer of Sb2S3 on nanocrystalline TiO_2 for $CH_3NH_3PbI_3$ perovskite solar cells *J. Phys. Chem.* C **118** 16995–7000
[129] Murugadoss G, Mizuta G, Tanaka S, Nishino H, Umeyama T, Imahori H and Ito S 2014 Double functions of porous TiO_2 electrodes on $CH_3NH_3PbI_3$ perovskite solar cells: enhancement of perovskite crystal transformation and prohibition of short circuiting *APL Mater.* **2** 081511
[130] O'Regan B and Lenzmann F 2004 Charge transport and recombination in a nanoscale interpenetrating network of n-type and p-type semiconductors: transient photocurrent and photovoltage studies of TiO_2/dye/CuSCN photovoltaic cells *J. Phys. Chem.* B **108** 4342–50
[131] O'Regan B, Scully S and Mayer A 2005 The effect of Al_2O_3 barrier layers in TiO_2/Dye/CuSCN photovoltaic cells explored by recombination and DOS characterization using transient photovoltage *J. Phys. Chem.* B **109** 4616–23
[132] Perera V P S, Pitigala P K D D P, Senevirathna M K I and Tennakone K 2004 A solar cell sensitized with three different dyes *Sol. Energy Mater. Sol. Cells* **85** 91–8
[133] Mahrov B, Hagfeldt A, Lenzmann F and Boschloo G 2005 Comparison of charge accumulation and transport in nanostructured dye-sensitized solar cells with electrolyte or CuSCN as hole conductor *Sol. Energy Mater. Sol. Cells* **88** 351–62
[134] Cole D and Bruck H 2005 Interfacial gradient for solid-state dye-sensitized solar cells, *2005 SEM Proc.* pp 4–7
[135] Gong J, Liang J and Sumathy K 2012 Review on dye-sensitized solar cells (DSSCs): fundamental concepts and novel materials *Renew. Sustain. Energy Rev.* **16** 5848–60
[136] Narayan M R 2011 Review: dye sensitized solar cells based on natural photosensitizers *Renew. Sustain. Energy Rev.* **16** 208–15
[137] Choi H, Nahm C, Kim J, Kim C, Kang S, Hwang T and Park B 2013 Review paper: Toward highly efficient quantum-dot- and dye-sensitized solar cells *Curr. Appl. Phys.* **13** S2–13
[138] Hagfeldt A, Boschloo G, Sun L, Kloo L and Pettersson H 2010 Dye-sensitized solar cells *Chem. Rev.* **110** 6595–663
[139] Listorti A, O'Regan B and Durrant J 2011 Electron transfer dynamics in dye-sensitized solar clls *Chem. Mater.* **23** 3381–99
[140] Zhang X, Wang S-T and Wang Z-S 2011 Effect of metal-doping in TiO_2 on fill factor of dye-sensitized solar cells *Appl. Phys. Lett.* **99** 113503
[141] Lee J-K and Yang M 2011 Progress in light harvesting and charge injection of dye-sensitized solar cells *Mater. Sci. Eng.* B **176** 1142–60
[142] Ning Z, Fu Y and Tian H 2010 Improvement of dye-sensitized solar cells: what we know and what we need to know *Energy Environ. Sci.* **3** 1170
[143] Hashmi G, Miettunen K, Peltola T, Halme J, Asghar I, Aitola K, Toivola M and Lund P 2011 Review of materials and manufacturing options for large area flexible dye solar cells *Renew. Sustain. Energy Rev.* **15** 3717–32
[144] Odobel F, Pellegrin Y, Gibson E A, Hagfeldt A, Smeigh A L and HamMarström L 2012 Recent advances and future directions to optimize the performances of p-type dye-sensitized solar cells *Coord. Chem. Rev.* **256** 2414–23
[145] Perera V P S, Senevirathna M K I, Pitigala P K D D P and Tennakone K 2005 Doping CuSCN films for enhancement of conductivity: application in dye-sensitized solid-state solar cells *Sol. Energy Mater. Sol. Cells* **86** 443–50
[146] Premalal E V A, Kumara G R R A, Rajapakse R M G, Shimomura M, Murakami K and Konno A 2010 Tuning chemistry of CuSCN to enhance the performance of TiO_2/N719/CuSCN all-solid-state dye-sensitized solar cell *Chem. Commun.* **46** 3360–2
[147] Premalal E V A, Dematage N, Kumara G R R A, Rajapakse R M G, Shimomura M, Murakami K and Konno A 2012 Preparation of structurally modified, conductivity enhanced-p-CuSCN and its application in dye-sensitized solid-state solar cells *J. Power Sources* **203** 288–96
[148] Premalal E V A, Dematage N and Konno A 2012 Carbon black paste combined with conductivity-enhanced CuSCN for improved performance in quasi-solid-state dye-sensitized solar cells *Chem. Lett.* **41** 510–2
[149] Li M-H, Shen P-S, Wang K-C, Guo T-F and Chen P 2015 Inorganic p-type contact materials for perovskite-based solar cells *J. Mater. Chem.* A **3** 9011–9
[150] Park N-G 2015 Perovskite solar cells: an emerging photovoltaic technology *Mater. Today* **18** 65–72
[151] Yin W-J, Yang J-H, Kang J, Yan Y and Wei S-H 2015 Halide perovskite materials for solar cells: a theoretical review *J. Mater. Chem.* A **3** 8926–42
[152] Yan J and Saunders B R 2014 Third-generation solar cells: a review and comparison of polymer:fullerene, hybrid polymer and perovskite solar cells *RSC Adv.* **4** 43286–314
[153] Kojima A, Teshima K, Shirai Y and Miyasaka T 2009 Organometal halide perovskites as visible-light sensitizers for photovoltaic cells *J. Am. Chem. Soc.* **131** 6050–1
[154] Loh L, Briscoe J and Dunn S 2013 Perovskite enhanced solid state ZnO solar cells *J. Phys. Conf. Ser.* **476** 012008
[155] Ye S, Sun W, Li Y, Yan W, Peng H, Bian Z, Liu Z and Huang C 2015 CuSCN-based inverted planar perovskite solar cell with an average PCE of 15.6% *Nano Lett.* **15** 3723–8
[156] Ito S, Tanaka S and Nishino H 2015 Substrate-preheating effects on PbI_2 spin coating for perovskite solar cells via sequential deposition *Chem. Lett.* **44** 849–51
[157] Ito S, Tanaka S and Nishino H 2015 Lead-halide perovskite solar cells by CH_3NH_3I-dripping on PbI_2-CH_3NH_3I-DMSO precursor layer for planar and porous structures using CuSCN hole transporting material *J. Phys. Chem. Lett.* **6** 881–6
[158] Baumann A, Väth S, Rieder P, Heiber M C, Tvingstedt K and Dyakonov V 2015 Identification of trap states in perovskite solar cells *J. Phys. Chem. Lett.* **6** 2350–4
[159] Wang J, Zhang F, Zhang J, Tang W, Tang A, Peng H, Xu Z, Teng F and Wang Y 2013 Key issues and recent progress of high efficient organic light-emitting diodes *J. Photochem. Photobiol.* C **17** 69–104
[160] Thejokalyani N and Dhoble S J 2014 Novel approaches for energy efficient solid state lighting by RGB organic light emitting diodes—a review *Renew. Sustain. Energy Rev.* **32** 448–67
[161] Wang Z B, Helander M G, Qiu J, Puzzo D P, Greiner M T, Hudson Z M, Wang S, Liu Z W and Lu Z H 2011 Unlocking the full potential of organic light-emitting diodes on flexible plastic *Nat. Photonics* **5** 753–7
[162] D'Andrade B W and Forrest S 2004 White organic light-emitting devices for solid-state lighting *Adv. Mater.* **16** 1585–95
[163] Reineke S, Lindner F, Schwartz G, Seidler N, Walzer K, Lüssem B and Leo K 2009 White organic light-emitting diodes with fluorescent tube efficiency *Nature* **459** 234–8

[164] Suzuki M, Fukagawa H, Nakajima Y, Tsuzuki T, Takei T, Yamamoto T and Tokito S 2009 A 5.8-in. phosphorescent color AMOLED display fabricated by ink-jet printing on plastic substrate *J. Soc. Inf. Disp.* **17** 1037–42

[165] Hofmann S, Thomschke M, Lussem B and Leo K 2011 Top-emitting organic light-emitting diodes *Opt. Express* **19** A1250–64

[166] Zhang Y and Forrest S 2012 Triplets contribute to both an increase and loss in fluorescent yield in organic light emitting diodes *Phys. Rev. Lett.* **108** 267404

[167] D'Andrade B 2012 Molecules that convert heat into light *Nature* **492** 197

[168] Xu L-J, Wang J-Y, Zhu X-F, Zeng X-C and Chen Z-N 2015 Phosphorescent cationic Au_4Ag_2 alkynyl cluster complexes for efficient solution-processed organic light-emitting diodes *Adv. Funct. Mater.* **25** 3033–42

[169] Xing X, Zhong L, Zhang L, Chen Z, Qu B, Chen E and Xiao L 2013 Essential differences of organic films at the molecular level via vacuum deposition and solution processes for organic light-emitting diodes *J. Phys. Chem.* C **117** 25405–8